1985

The Incorporation Of Titanium In Phlogopite In A Simplified, Synthetic System: A Potential Geothermobarometer For Upper Mantle And Lower Crustal Rocks

Reidar Gjermund Tronnes

CANADIAN THESES ON MICROFICHE

I.S.B.N.

THESES CANADIENNES SUR MICROFICHE

National Library of Canada
Collections Development Branch

Canadian Theses on
Microfiche Service

Ottawa, Canada
K1A 0N4

Bibliothèque nationale du Canada
Direction du développement des collections

Service des thèses canadiennes
sur microfiche

NOTICE

The quality of this microfiche is heavily dependent upon the quality of the original thesis submitted for microfilming. Every effort has been made to ensure the highest quality of reproduction possible.

If pages are missing, contact the university which granted the degree.

Some pages may have indistinct print especially if the original pages were typed with a poor typewriter ribbon or if the university sent us a poor photocopy.

Previously copyrighted materials (journal articles, published tests, etc.) are not filmed.

Reproduction in full or in part of this film is governed by the Canadian Copyright Act, R.S.C. 1970, c. C-30. Please read the authorization forms which accompany this thesis.

AVIS

La qualité de cette microfiche dépend grandement de la qualité de la thèse soumise au microfilmage. Nous avons tout fait pour assurer une qualité supérieure de reproduction.

S'il manque des pages, veuillez communiquer avec l'université qui a conféré le grade.

La qualité d'impression de certaines pages peut laisser à désirer, surtout si les pages originales ont été dactylographiées à l'aide d'un ruban usé ou si l'université nous a fait parvenir une photocopie de mauvaise qualité.

Les documents qui font déjà l'objet d'un droit d'auteur (articles de revue, examens publiés, etc.) ne sont pas microfilmés.

La reproduction, même partielle, de ce microfilm est soumise à la Loi canadienne sur le droit d'auteur, SRC 1970, c. C-30. Veuillez prendre connaissance des formules d'autorisation qui accompagnent cette thèse.

THIS DISSERTATION
HAS BEEN MICROFILMED
EXACTLY AS RECEIVED

LA THÈSE A ÉTÉ
MICROFILMÉE TELLE QUE
NOUS L'AVONS REÇUE

NL-339 (r. 82/08)

Canada

THE INCORPORATION OF Ti IN PHLOGOPITE IN A SIMPLIFIED, SYNTHETIC SYSTEM: A POTENTIAL GEOTHERMOBAROMETER FOR UPPER MANTLE AND LOWER CRUSTAL ROCKS

by

Reidar Gjermund Trønnes

Department of Geology

Submitted in partial fulfillment
of the requirements for the degree of
Doctor of Philosophy

Faculty of Graduate Studies
The University of Western Ontario
London, Ontario
January, 1985

ABSTRACT

The solubility of Ti in phlogopite has been experimentally determined in the system $K_2Mg_6Al_2Si_6O_{20}(OH)_4$-$K_2Mg_4TiAl_2Si_6O_{20}(OH)_4$-$K_2Mg_5TiAl_4Si_4O_{20}(OH)_4$ from 10 to 30 kbar and from 825 to 1300°C. Starting compositions along the join $K_2Mg_6Al_2Si_6O_{20}(OH)_4$-$K_2Mg_{4.5}TiAl_3Si_5O_{20}(OH)_4$ were used in order to evaluate the relative importance of the two substitution mechanisms $2Mg = Ti$ and $Mg(2Si)^{IV} = Ti(2Al^{IV})$. These two substitution mechanisms are represented by the joins from the phlogopite molecule ($K_2Mg_6Al_2Si_6O_{20}(OH)_4$) to the Ti-OSD (Octahedral Site Deficiency) molecule ($K_2Mg_4TiAl_2Si_6O_{20}(OH)_4$) and to the Ti-eastonite molecule ($K_2Mg_5TiAl_4Si_4O_{20}(OH)_4$), respectively.

The solubility of Ti in phlogopite increases with increasing temperature and decreases with increasing pressure. For a given starting composition the Ti-OSD/Ti-eastonite and the eastonite/phlogopite ratios in the phlogopite solid solution coexisting with rutile increase with decreasing Ti-content of the phlogopite. The variations in the proportions of the phlogopite and the Ti-OSD end members with variations in temperature and pressure are minor.

The compositions of the experimentally produced phlogopites in terms of the relative proportions of the end member molecules are similar to the compositions of phlogo-

pites from mantle xenoliths, mantle derived, mafic and ultramafic igneous rocks and lower crustal granulites. Based on the experimental data, compositional diagrams including the two Ti-rich phlogopite end members and the sum of the Ti-free end members were contoured for temperature (isobaric diagrams) and pressure (isothermal diagrams). The application of such a phlogopite geothermobarometer to phlogopites from mantle xenoliths and lower crustal granulites gives temperatures and pressures in good agreement with the temperatures and pressures determined by independent geothermometers and geobarometers. The accuracy of the temperature determinations is better than that of the pressure determinations.

Since the geothermobarometer is based on a subsolidus experimental study, it can not be applied to phlogopites that crystallized from a melt. Although further refinements of the phlogopite geothermobarometer are needed, the relationships derived from the simplified experimental system form a basis for determining the physical conditions of phlogopite formation in the upper mantle and the lower crust.

ACKNOWLEDGEMENTS

This work was carried out under the supervision of Dr. Alan D. Edgar. I would like to thank him for his guidance and constructive criticism. Dr. M. Arima contributed a wealth of ideas and provided very helpful advice during the experimental and analytical work. Dr. W.R. Church gave access to his personal computer facilities, and introduced me to BASIC programming. Dr. A. Kishida provided additional programming assistance.

Technical assistance was provided by R. Shirran (high pressure experimental laboratory), Y. Cheng (X-ray diffraction lab), J. Forth (preparation of thin sections) and R.L. Barnett (electron microprobe lab). G. McIntyre typed the manuscript, and M. MacLeod and A. Noon prepared the figures. The study was supported by fellowships (1981/82 and 1982/83) from Norges Teknisk-Naturvitenskapelige Forskningsrad and teaching assistantships (1983/84 and 1984 fall term) from the University of Western Ontario. The experimental and analytical expenses were covered by an operating grant from the Natural Sciences and Engineering Research Council of Canada to Dr. A.D. Edgar.

TABLE OF CONTENTS

LIST OF TABLES

LIST OF FIGURES

LIST OF APPENDICES

CHAPTER 1

INTRODUCTION

1.1 Significance of phlogopite in the mantle

Phlogopite is present as a widespread, but minor, constituent in parts of the upper mantle to depths of 150-200 km (Modreski & Boettcher, 1972; Carswell, 1975; Delaney et al., 1980). To a very limited extent the mineral also occurs in large quantities, often along with clinopyroxene, in veins and irregular patches presumably as a result of mantle metasomatism (Dawson & Smith, 1977; Lloyd & Bailey, 1975; Boettcher et al., 1979; Bailey, 1982; Harte, 1983).

At least two textural types of phlogopite have been identified in ultramafic xenoliths brought to the surface by alkali basalts, kimberlites and ultrapotassic lavas (Carswell, 1975; Delaney et al., 1980). Coarse grained, primary phlogopite is in textural equilibrium (see Carswell, 1975) with the coexisting anhydrous silicates, whereas fine grained, secondary phlogopite occurs in

criss-crossing veins or as alteration fringes on garnet, orthopyroxene, clinopyroxene and primary phlogopite (Carswell, 1975; Boettcher and O'Neil, 1980; Delaney et al., 1980). The primary phlogopite grains are commonly kink-banded and deformed, and are considered to have equilibrated with the surrounding mineral assemblage. The textural relations of the often completely undeformed secondary phlogopite grains indicate that they formed by metasomatism or by a reaction with, or crystallization from, a melt (Dawson & Smith, 1977; Boettcher et al., 1979).

In a series of papers, Sekine & Wyllie (1982a,b,c, 1983) and Wyllie & Sekine (1982) proposed that phlogopite will form in the mantle wedge above subduction zones as a result of hybridization between a hydrous, siliceous magma, produced by melting of the slab, and the overlying hotter peridotite. Several authors have also emphasized the importance of phlogopite as a component in the source regions of ultrapotassic and kimberlitic melts in the continental lithosphere (e.g. Edgar et al., 1976; Wyllie, 1979; Wendlandt & Eggler, 1980a,b; Pasteris, 1981, 1984; Arima & Edgar, 1983a,b; McCulloch et al., 1983; Smith, 1983).

Phlogopite, and to some extent potassium richterite and other amphiboles, represent the most important sources of potassium in the upper mantle (e.g. Dawson & Smith,

1982). In addition phlogopite is a major reservoir for water and halogens (especially flourine), as well as for large ion lithophile elements such as Rb, Cs and Ba (Smith et al., 1979, 1981).

1.2 Purpose and scope

Phlogopite present in mantle xenoliths, alkali basalts, ultrapotassic and kimberlitic rocks and in granulite facies rocks of the lower continental crust, commonly has high, but variable, titanium contents (e.g. Boettcher & O'Neill, 1980; Van Kooten, 1980; Clifford et al., 1981; Ehrenberg, 1982; Griffin et al., 1979, 1984; Mitchell, 1981, 1984; Bachinski & Simpson, 1984; Irving and Frey, 1984). Arima & Edgar (1981) suggested that the titanium solubility in phlogopite occurring in mantle derived xenoliths and ultrapotassic rocks may be a potential geothermometer and/or geobarometer. The main objective of the present study is to determine the variation in the solubility of titanium in simplified phlogopite compositions as a function of pressure and temperature under conditions corresponding to the uppermost part of the upper mantle (10-30 kbar, 825-1375°C).

Because the substituion of titanium in phlogopite also involves changes in the proportions of the other major elements (especially Mg, Al and Si), the contents of these elements must also be considered in an evaluation of the

incorporation of titanium in phlogopite.

The investigation was carried out by crystallizing phlogopite from simplified synthetic starting materials under controlled physical conditions. The results from the experimental study of the variation of the titanium solubility in phlogopite are compared with chemical data on phlogopite from various occurrences of ultrapotassic rocks, lamprophyres, kimberlites, mantle derived xenoliths and lower crustal granulites. Based on established geothermometers and geobarometers in these rocks, the applicability of Ti-solubility in phlogopite as a geothermobarometer has been assessed.

1.3 Cation substitutions in the trioctahedral mica group

Dymek (1983) gives a summary of the most important cation substitutions in the various crystallographic sites in trioctahedral mica. Changes in mica composition, including the incorporation of Ti in the mineral, are dominantly associated with the octahedral and tetrahedral sites. However, some substitutions involving the large 12-coordinated interlayer sites and the hydroxyl and halogen sites may in some cases play an important role in phlogopites in rocks of mantle origin. For instance, a decrease in the Si/Al ratio in the tetrahedral sites may take place in response to the substitution of Ba and Ca for K in the interlayer site. The substitution of Al and Ti

for Mg and Fe in octahedral sites may accompany substitution of O^{2-} for OH^- (Bohlen et al., 1980).

In phlogopites from the Shaw's Cove minette, Bachinski & Simpson (1984) found a positive correlation between K and Si along with a considerable deficiency of typical interlayer cations and an excess of the cations normally considered to occupy the octahedral sites. They attributed these features to the substitution $K^{XII} + Si^{IV} = (Mg,Fe^{2+})^{XII} + Al^{IV}$. Other phlogopites may have compositions characterized by octahedral Al coupled with K-deficiency or by octahedral and interlayer site vacancies accompanied by substitution of Ba and Ca for K. However, as pointed out by Wendlandt (1977) and Gaspar & Wyllie (1982), the main charge compensation for the incorporation of Ba and Ca in phlogopite is provided by a coupled substitution of Al^{IV} for Si.

Two of the most common cation substitutions in the trioctahedral mica series are the $Mg^{VI} = Fe^{VI}$ substitution (phlogopite-annite) and the $Mg^{VI}Si^{IV} = Al^{VI}Al^{IV}$ substitution (phlogopite-eastonite). Foster (1960a,b) also suggested that additional Al is incorporated by a dioctahedral-trioctahedral substitution (biotite-muscovite).

Several different substitution processes have been suggested for the incorporation of Ti into phlogopite (Arima & Edgar, 1981; Dymek, 1983). Kunitz (1936) proposed

a tetrahedral substitution of Ti^{4+} for Si^{4+}. This mechanism is of potential importance in phlogopites where (Si+Al)<8 (number of cations normalized to a total charge of 44). Farmer & Boettcher (1981) found that ferric iron enters the tetrahedral site only if (Si+Al+Ti)<8 to produce reverse pleochroism of the phlogopites. In phlogopites with (Si+Al)<8< (Si+Al+Ti) titanium and not ferric iron should therefore enter the tetrahedral site. However, tetrahedral Fe^{3+} is often present in considerable amounts in phlogopites (Wones et al., 1971; Burns & Dyar, 1984), and Wendlandt (1977) and Arima & Edgar (1981) found evidence that Fe^{3+} may enter the tetrahedral site in preference to Ti in phlogopites.

Engel & Engel (1960) suggested that titanium may be present as Ti^{3+} and may replace Al^{3+} in octahedral sites, and based on an X-ray photoelectron study, Evans and Raftery (1980) concluded that Ti^{3+} was present in the biotites they investigated. However, optical spectra of trioctahedral micas have not confirmed the presence of Ti^{3+} (Faye, 1968; Burns & Vaughan, 1975). As pointed out by Dymek (1983), most biotites and phlogopites in natural rocks coexist with oxides (e.g. rutile and ilmenite) and other minerals where titanium is present as Ti^{4+}. Comparison of electron energy-loss spectra for biotite and amphibole with rutile, ilmenite, titanite and Ti-omphacite has also shown that the oxidation state of Ti is identical

in all of these minerals (Otten, 1984).

Two important substitution mechanisms seem to account for the largest proportion of titanium in phlogopite. The first, and apparently the most common substitution in phlogopite crystallized under high pressure, is $(2Mg)^{VI} = (Ti)^{VI}$. This substitution, later referred to as the octahedral site deficiency (OSD) substitution, was favoured by Forbes & Flower (1974) and Dymek (1983).

The second important mechanism involves a replacement of octahedral divalent cations (mainly Mg) by Ti^{4+} coupled with a replacement of Si by Al on tetrahedral site. This substitution ($Mg^{VI}{}_2Si^{IV} = Ti^{VI}{}_2Al^{IV}$) leads to the Ti-eastonite end member $K_2(Mg_5Ti)^{VI}(Si_4Al_4)^{IV}O_{20}(OH)_4$. It appears that this mechanism plays a greater role in phlogopites and biotites with high titanium content crystallized under upper crustal pressure conditions (e.g. Czamanske & Wones, 1973; Robert, 1976; Guidotti et al., 1977).

In trioctahedral mica containing Al in octahedral coordination, Ti may also be incorporated by the substitution $(2Al)^{VI} = (MgTi)^{VI}$. Bohlen et al. (1980) and Abrecht and Hewitt (1980, 1981) suggested that combinations of all three mechanisms mentioned must be invoked to explain their data. Most of the phlogopites found in kimberlites, ultrapotassic rocks and their mantle xenoliths, as well as in the phlogopites crystallized in high pressure experiments

performed on ultrapotassic rock compositions, are characterized by large proportions of the Ti-OSD and the Ti-eastonite end members (Arima & Edgar, 1981).

1.4 Choice of system

In order to evaluate the solubility of Ti in phlogopite experimentally while avoiding the additional effects of elements such as Na, Ba, Fe, Mn, Ca, F and Cl, compositions in the system K_2O-MgO-Al_2O_3-SiO_2-TiO_2-H_2O were chosen (Fig. 1). As pointed out by Arima and Edgar (1981) most of the compositional variation of Ti-rich phlogopites may be explained by the substitution processes $2Mg^{VI} = (Ti\ )^{VI}$ and $Mg^{VI}(2Si)^{IV} = Ti^{VI}(2Al)^{IV}$. To study the relative effects of these substitutions, compositions along the join from $K_2Mg_{4.5}TiAl_3Si_5O_{20}(OH)_4$ to the phlogopite corner in Fig. 1 were used as starting compositions. A few exploratory runs were also carried out with the end member compositions Ti-OSD and Ti-eastonite as starting materials. The compositions of the starting materials are listed in Table 1.

Figure 1. Starting material compositions in the system $K_2Mg_6Al_2Si_6O_{20}(OH)_4$-$K_2Mg_4TiAl_2Si_6O_{20}(OH)_4$-$K_2Mg_5TiAl_4Si_4O_{20}(OH)_4$. The chemical compositions of the starting materials are listed in Table 1.

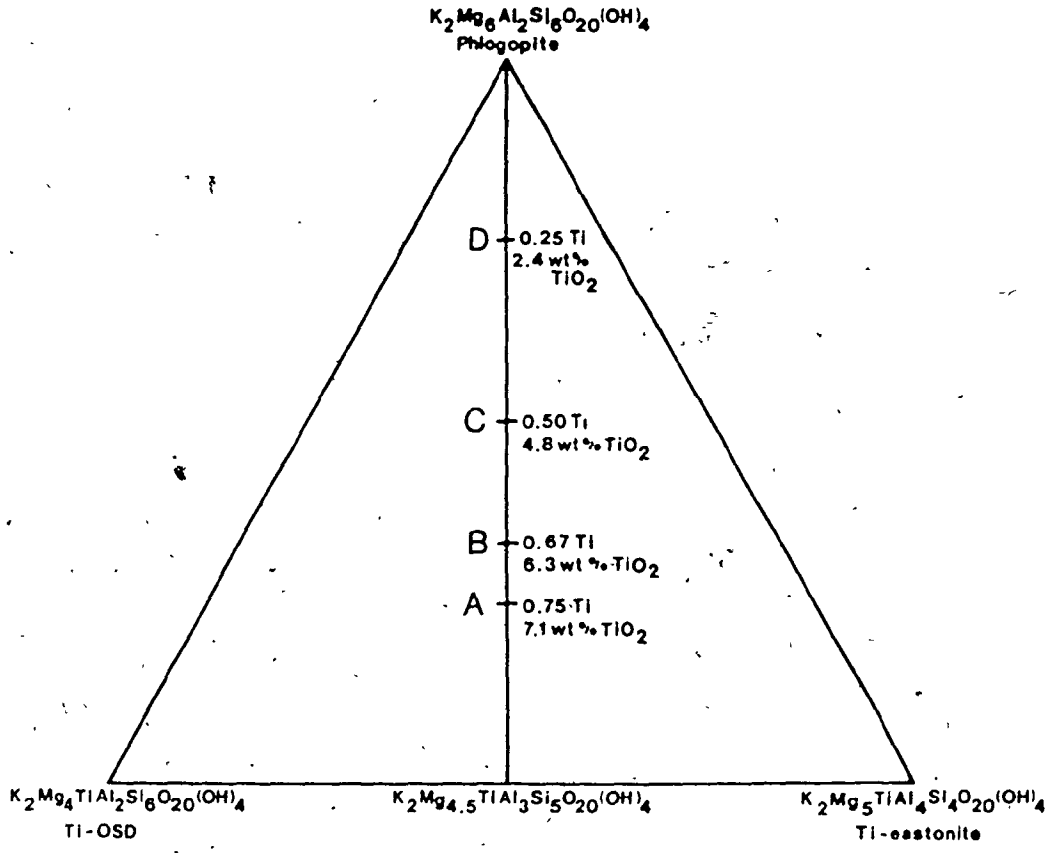
$K_2Mg_6Al_2Si_6O_{20}(OH)_4$
Phlogopite
D
0.25 Ti
2.4 wt% TiO_2
C
0.50 Ti
4.8 wt% TiO_2
B
0.67 Ti
6.3 wt% TiO_2
A
0.75 Ti
7.1 wt% TiO_2
$K_2Mg_4TiAl_2Si_6O_{20}(OH)_4$
Ti-OSD
$K_2Mg_{4.5}TiAl_3Si_5O_{20}(OH)_4$
$K_2Mg_5TiAl_4Si_4O_{20}(OH)_4$
Ti-eastonite

Table 1. Compositions of phlogopite end members and starting materials.

Wt. %	Phlog	East	Ti-east	Ti-OSD	Comp. A	Comp. B	Comp. C	Comp. D
SiO_2	43.20	35.93	28.08	43.23	37.47	38.08	39.35	41.26
Al_2O_3	12.22	24.39	23.82	12.23	16.65	16.16	15.18	13.70
TiO_2	-	-	9.33	9.58	7.12	6.33	4.76	2.39
MgO	28.98	24.11	23.55	19.34	23.28	23.95	25.20	27.09
K_2O	11.28	11.27	11.01	11.30	11.19	11.20	11.21	11.25
H_2O	4.32	4.31	4.21	4.32	4.28	4.28	4.29	4.30
Sum	100.00	100.01	100.00	100.00	99.99	100.00	99.99	100.00

Cations normalized to a total charge of 44 (22 oxygen atoms)

Si	6.000	5.000	4.000	6.000	5.250	5.333	5.500	5.750
Al^{IV}	2.000	3.000	4.000	2.000	2.750	2.667	2.500	2.250
Al^{VI}	-	1.000	-	-	-	-	-	-
Ti	-	-	1.000	1.000	0.750	0.667	0.500	0.250
Mg	6.000	5.000	5.000	4.000	4.875	5.000	5.250	5.625
OSO	6.000	6.000	6.000	5.000	5.625	5.667	5.750	5.875
OSD	-	-	-	1.000	0.375	0.333	0.250	0.125
K	2.000	2.000	2.000	2.000	2.000	2.000	2.000	2.000
H	4.000	4.000	4.000	4.000	4.000	4.000	4.000	4.000

OSO: octahedral site occupancy. OSD: octahedral site deficiency (relative to 6 octahedrally coordinated cations). Phlog: pure Mg-phlogopite end member. East: eastonite end member. Ti-east: Ti-rich end member formed from Phlog by the substitution Mg2Al = Ti2Si, and containing one Ti cation per 22 O (or 20 O + 4(OH)). Ti-OSD: Ti-rich octahedral site deficient end member formed from Phlog by the substitution 2 Mg = Ti , and containing one Ti cation per 22 O (or 20 O + 4(OH)).

CHAPTER 2

EXPERIMENTAL AND ANALYTICAL METHODS

2.1 Starting materials

The anhydrous phlogopite compositions used in this study were prepared from oxide mixtures. The decision to use oxide mixtures instead of a potentially more reactive material was made on the basis of the greater complexities and sources of compositional errors associated with the preparation of gels and glasses. Specifically, gels tend to nucleate metastable phases both during preparation and experimental runs. It is also difficult to control the composition and homogeneity of gels, and loss of alkalies by volatilization may be a serious problem in the preparation of both gels and glasses.

Although most of the experiments were performed under subsolidus conditions, the problem of reduced reactivity was considered to be minor due to the fact that the system is hydrous. Experiments with run durations varying from 5

to 13 hours (Table 2) in the stability range of a single phase phlogopite solid solution containing about 6 wt. % TiO_2 have indicated that TiO_2, which presumably is the most refractory component, reacts completely within run durations of less than 5 hrs at 1200°C and less than 6 hrs at 1000°C.

The attainment of equilibrium and the location of the solubility limit of TiO_2 in phlogopite for composition B (Table 1) have been confirmed by reversing two of the runs across the solubility line (Table 2; Fig. 2). Appendix 1 lists the oxide and carbonate components and their treatment before they were weighed out to form the anhydrous phlogopite compositions of Table 1. The further procedure for the preparation of the starting materials is also outlined in Appendix 1.

2.2 High pressure experiments

The procedures for preparing the sample capsules ($Ag_{50}Pd_{50}$ and Pt) are given in Appendix 2. The high pressure experiments were carried out using a 1.27 cm piston-cylinder apparatus (Boyd & England, 1960) with talc and pyrex glass as the pressure transmitting media. Talc-boron nitride assemblies were used for some of the runs at 10 kbar.

The "hot piston out" technique (see e.g. Johannes, et al., 1971) was used. Pressure and temperature were cali-

brated at the kyanite = sillimanite transition at 22 kbar and 1300°C (Richardson et al., 1968), at the albite = jadeite + quartz transition at 16.3 kbar and 600°C (Johannes et al., 1971; Holland, 1980), and at the melting point of diopside at 10 kbar and 1530°C (Boyd & England, 1960). Both pressure and temperature were within the accepted range of values for the transformations based on interlaboratory comparisons (Johannes et al., 1971). No frictional correction was made for pressure, and no pressure correction to the e.m.f. of the $Pt-Pt_{90}Rh_{10}$ thermocouple was made. The pressure and temperature can be controlled to within $\pm$ 0.5 kbar and $\pm$ 10°C, respectively. The graphite furnace assemblage buffers the f_{H_2} in the sample capsule corresponding to f_{O_2} values close to the NNO buffer (Brey & Green, 1977).

2.3 Identification and analysis of run products

After each run contamination was removed from the surface of the capsule before weighing and opening. Accidental water loss from the capsule during a run was detected by a combination of a significant weight loss (2.10^{-4} to 3.10^{-4} g) and an extremely hard and fine grained, anhydrous run product. When sufficient water was present to form stoichiometric phlogopite, the run products were soft and relatively coarse grained, comprising well crystallized, hexagonally outlined thin plates of phlogo-

pite (10 to 100 μm across) and tiny needles of rutile.

No weight loss was detected by reweighing of the capsules and contents after heating them to about 110°C for about 15 min subsequent to opening. This indicates that the amount of free vapour, if present, is very small in all of the runs. The minerals present in the run products were identified by optical examination in immersion oils. The phlogopite compositions were determined by electron microprobe on carbon coated polished thin sections. The instrument specifications and the operating conditions are given in Appendix 3.

2.4 Estimation of experimental and analytical compositional uncertainties

The weighing out of the anhydrous phlogopite compositions (totals of 5-10 g for each composition) is not considered to involve any source of significant compositional errors. However, the amount of H_2O required in each sample capsule to form a stoichiometric phlogopite composition is only 0.27 mg (4.3 wt. % H_2O) corresponding to 6 mg of anhydrous powder (see Appendix 2). The weighing operation is characterized by an uncertainty of $\pm$ 0.02 to $\pm$ 0.03 mg. This may lead to an uncertainty in the proportion of H_2O of about 4.3 $\pm$ 0.4 wt. % (Appendix 2).

The precision of the electron microprobe analyses estimated from repeated analyses of phlogopites from

various run products is generally better than ± 1.0 wt. % (1 standard deviation) for SiO_2, ± 0.8 wt. % for Al_2O_3 and MgO and ± 0.3 wt. % for TiO_2 and K_2O. The accuracy estimated from analyses of standards appears to be equivalent with the precision.

CHAPTER 3

EXPERIMENTAL RESULTS

The results of the experiments and the chemical compositions of the phlogopites are listed in Table 2. Compositional homogeneity of the phlogopite, both within the same grain and between grains was indicated by single spot analyses. The analyses reported in Table 2 represent averages of 1 to 3 spot analyses of 3 to 10 grains for each experimental run.

Fig. 2 shows the variation in the TiO_2-contents of the phlogopites and the mineral assemblages as a function of pressure and temperature for the starting compositions A, B, C and D (Fig. 1). The TiO_2-content of the phlogopites coexisting with rutile increases with increasing temperature (at constant pressure) and decreases with increasing pressure (at constant temperature) for all compositions.

Table 2. Experimental results and chemical composition of the produced phlogopites.

Composition	A	A	A	A	A	A	A	A	A	A	A	A
Pressure(kbar)	10	15	20	30	15	30	10	15	15	15	30	15
Temperature(°C)	1000	1000	1000	1000	1100	1100	1050	1150	1175	1200	1200	1250
Run time (hrs)	6.5	7.5	6	6.5	6	8	6	6	8	6	7.5	6
Coexisting phase	Ru	Ru	Ru	Ru	Ru	Ru	-	Ru	-	Fo+gl	Ru	Fo+gl
SiO_2	37.4	38.3	39.3	39.2	40.8	39.1	37.6	38.4	38.9	37.4	39.0	38.9
Al_2O_3	16.8	17.5	17.4	16.6	14.1	17.4	16.6	17.7	16.6	17.0	17.1	17.1
TiO_2	6.7	6.0	4.2	3.6	6.1	3.8	7.1	6.3	7.3	6.4	4.7	6.3
MgO	23.7	23.2	23.3	23.3	23.8	24.7	23.3	23.2	22.9	24.0	23.4	23.2
K_2O	11.1	10.7	10.5	10.7	11.0	11.1	11.0	10.7	10.6	11.1	10.8	10.5
Sum	95.7	95.7	94.7	93.4	95.8	96.1	95.6	96.3	96.3	95.9	95.0	96.0
Si	5.241	5.334	5.504	5.577	5.678	5.429	5.264	5.322	5.382	5.233	5.459	5.388
Al	2.759	2.666	2.496	2.423	2.311	2.571	2.736	2.678	2.618	2.767	2.541	2.612
Al[1]	0.018	0.209	0.378	0.356	[0.011]	0.270	0.014	0.206	0.088	0.033	0.276	0.182
Ti	0.705	0.629	0.442	0.383	0.625	0.399	0.746	0.652	0.762	0.675	0.497	0.660
Mg	4.953	4.806	4.857	4.939	4.934	5.105	4.874	4.781	4.714	4.997	4.895	4.783
OSO	5.676	5.644	5.677	5.678	5.559	5.774	5.634	5.639	5.564	5.705	5.668	5.625
K	1.976	1.908	1.879	1.946	1.944	1.955	1.962	1.889	1.876	1.974	1.934	1.862
Ti-OSO	33.8	40.9	38.8	34.3	48.1	24.6	39.2	42.9	52.4	31.1	36.4	46.6
Ti-eastonite	37.4	23.3	6.0	3.3	16.1	14.9	36.8	24.3	27.9	37.0	13.2	22.5
Phlogopite	26.7	11.8	12.1	23.0	35.6	30.5	22.5	8.9	9.2	28.1	19.3	9.4
Eastonite[2]	2.1	24.0	43.1	39.4	[0.20]	30.0	1.6	23.9	10.5	3.7	31.0	21.4

Appendix 4 reviews the calculation of structural formulae (22 O-atoms) and end member molecules. [1]: Numbers in brackets represent tetrahedral Ti when no octahedral Al is present. [2]: Numbers in bracket represent the tetrahedral Ti molecule when no eastonite is present. Coexisting phases: Rutile (Ru), Forsterite (Fo), glass (gl). Reversed experiments are indicated as (rev), and both the initial (highest) and final temperatures (lowest) are given.

Table 2. Cont.

Composition	A	A	A	A	A(glass)	A(glass)	B	B	B	B	B	B
Pressure(kbar)	25	30	30	30	15	30	10	15	20	25	30	15
Temperature(°C)	1250	1275	1300	1375	1200	1375	1000	1000	1000	1000	1000	1070
Run time (hrs)	6	6	7	6	6	6	9	10.5	7	6	6	10.5
Coexisting phase	-	-	Fo+gl	Fo+gl	Ph+Fo	Ph+Fo	Ru	Ru	Ru	Ru	Ru	Ru
SiO_2	37.9	38.4	37.6	37.9	38.6	39.5	37.7	38.2	39.0	39.7	39.8	37.9
Al_2O_3	17.0	16.3	17.5	17.7	16.5	18.1	16.5	16.5	16.5	17.2	16.9	16.2
TiO_2	7.1	7.2	6.8	6.4	7.8	7.9	5.6	5.1	4.4	4.5	3.0	6.3
MgO	23.3	23.3	22.7	22.8	15.2	15.5	24.1	23.6	24.0	23.7	24.4	23.5
K_2O	10.5	10.5	11.1	10.5	12.0	11.4	10.6	10.8	11.1	10.9	11.2	11.0
Sum	95.8	95.7	95.7	95.3	90.1	92.4	94.5	94.2	95.0	96.0	95.3	94.9
Si	5.279	5.347	5.262	5.303			5.331	5.413	5.476	5.500	5.557	5.349
Al	2.721	2.653	2.738	2.697			2.669	2.587	2.524	2.500	2.443	2.651
Al[1]	0.068	0.027	0.147	0.218			0.072	0.161	0.202	0.300	0.342	0.039
Ti	0.741	0.758	0.715	0.667			0.596	0.584	0.466	0.473	0.313	0.669
Mg	4.840	4.838	4.728	4.748			5.075	4.981	5.036	4.892	5.086	4.939
OSO	5.649	5.623	5.590	5.633			5.743	5.726	5.704	5.665	5.741	5.647
K	1.872	1.863	1.979	1.876			1.917	1.950	1.981	1.926	1.994	1.980
Ti-OSO	43.9	47.6	41.6	44.3			30.8	33.6	30.0	37.2	25.2	36.5
Ti-eastonite	34.6	33.4	29.3	24.8			30.8	21.4	15.8	10.0	4.9	30.7
Phlogopite	13.4	15.7	12.6	5.4			30.0	26.7	31.7	19.1	32.9	28.3
Eastonite[2]	8.1	3.3	16.4	25.4			8.4	18.2	22.4	33.7	37.0	4.4

Table 2. Cont.

Composition	B	B	B(r)	B	B(r)	B	B	B	B	B	B	B	B
Pressure(kbar)	25	30	20	20	25	20	25	30	20	30	30	25	30
Temperature(°C)	1070	1070	1150-1080	1100	1150-1100	1150	1150	1150	1200	1200	1215	1225	1225
Run time (hrs)	6	6	6+6	16	6+6	6	7	6	7	5	8	7	6
Coexisting phase	Ru	Ru	Ru	Ru	Ru	-	-	Ru	-	-	-	-	-
SiO_2	37.8	39.5	38.5	37.2	39.7	37.5	38.4	38.2	38.3	37.9	39.0	39.0	38.1
Al_2O_3	16.2	17.5	16.4	17.7	17.6	17.0	16.5	15.8	16.4	16.3	16.1	16.1	16.7
TiO_2	5.2	4.1	5.8	6.0	5.0	6.3	6.3	5.7	6.1	6.1	6.2	6.2	6.1
MgO	24.1	23.9	24.5	23.8	24.6	23.9	23.6	25.1	24.0	23.5	23.5	23.6	23.9
K_2O	10.7	10.7	11.5	10.7	10.9	10.8	11.0	10.8	10.8	10.9	10.7	10.6	10.7
Sum	94.0	95.7	96.7	95.4	97.8	95.5	95.8	95.6	95.6	94.7	95.5	95.5	95.5
Si	5.375	5.480	5.344	5.209	5.402	5.249	5.360	5.350	5.357	5.355	5.452	5.437	5.326
Al	2.625	2.520	2.656	2.791	2.598	2.751	2.640	2.605	2.643	2.645	2.548	2.563	2.674
Al[1]	0.088	0.340	0.021	0.138	0.222	0.058	0.007	[0.045]	0.054	0.062	0.098	0.082	0.070
Ti	0.551	0.430	0.602	0.628	0.515	0.666	0.663	0.554	0.641	0.649	0.646	0.654	0.646
Mg	5.105	4.942	5.074	4.987	4.994	4.987	4.902	5.231	5.000	4.953	4.884	4.904	4.985
OSO	5.744	5.712	5.697	5.744	5.731	5.711	5.642	5.785	5.695	5.664	5.628	5.640	5.701
K	1.947	1.896	2.040	1.908	1.884	1.938	1.952	1.952	1.920	1.955	1.902	1.892	1.909
Ti-OSO	28.7	34.3	28.3	31.1	33.7	32.7	38.7	25.6	35.8	36.3	43.8	43.2	35.7
Ti-eastonite	27.3	9.1	31.7	33.6	19.4	35.5	28.5	32.0	30.5	29.5	23.3	25.2	31.3
Phlogopite	34.0	18.0	37.7	19.3	21.1	25.1	23.9	41.6	27.5	27.0	21.4	22.0	24.7
Eastonite[2]	10.0	38.6	2.3	16.0	25.8	6.7	8.8	[0.8]	6.2	7.1	11.5	9.6	8.2

Table 2. Cont.

Composition	C	C	C	C	C	C	D	D	D	D	D	D
Pressure(kbar)	10	10	10	15	20	30	15	20	25	30	15	30
Temperature(°C)	850	900	950	950	950	950	825	825	825	825	900	900
Run time (hrs)	10	12	8	8	10	10	20	12	12	12	13	12
Coexisting phase	Ru	Ru	-	Ru	Ru	Ru	Ru	Ru	Ru	Ru	-	Ru
SiO_2	40.0	39.8	39.4	39.7	40.0	40.1	41.4	42.0	42.2	42.5	40.8	39.6
Al_2O_3	15.7	15.7	15.1	15.5	15.5	16.5	14.0	13.7	13.8	13.7	13.9	15.8
TiO_2	4.1	4.3	4.8	4.5	4.1	2.6	1.1	0.6	0.4	0.3	2.1	0.8
MgO	24.3	25.1	25.1	24.7	24.6	25.3	27.2	27.4	27.6	27.6	27.6	26.8
K_2O	11.2	11.1	10.8	11.2	10.9	10.8	10.0	10.8	11.0	10.8	11.0	10.3
Sum	95.3	96.0	95.2	95.6	95.1	95.3	93.7	94.5	93.2	94.9	95.4	93.3
Si	5.595	5.529	5.521	5.543	5.604	5.583	5.832	5.891	5.896	5.927	5.697	5.629
Al	2.405	2.471	2.479	2.457	2.396	2.417	2.168	2.109	2.104	2.073	2.289	2.371
Al[T]	0.180	0.107	0.014	0.091	0.152	0.295	0.152	0.151	0.169	0.182	[0.014]	0.277
Ti	0.436	0.447	0.501	0.477	0.433	0.276	0.117	0.065	0.041	0.031	0.207	0.081
Mg	5.065	5.198	5.252	5.139	5.128	5.250	5.724	5.733	5.738	5.736	5.754	5.676
OSO	5.681	5.753	5.767	5.707	5.713	5.821	5.993	5.949	5.948	5.949	5.961	6.034
K	1.991	1.965	1.93	1.997	1.952	1.927	1.796	1.929	1.958	1.93	1.954	1.864
Ti-OSO	31.8	26.6	27.8	29.2	31.2	21.5	10.9	6.5	4.1	3.1	6.2	3.3
Ti-eastonite	11	18.3	18.3	18.1	12.2	6.1	0.8	-	-	-	14.9	4.6
Phlogopite	37.3	43	43	42.6	39.3	3.93	71.2	78.5	79.0	72.1	78.7	62.1
Eastonite[2]	19.9	12.1	1.6	10.2	17.2	33.2	17.1	15.0	16.9	24.8	[0.2]	30.1

Table 2. Cont.

Composition	D	D	D	D	Ti-OSD	Ti-OSD	Ti-east
Pressure(kbar)	15	15	20	30	20	30	20
Temperature(°C)	950	1000	1000	1000	1150	1150	1100
Run time (hrs)	13	6	6	10	7.5	6	7.5
Coexisting phase	-	-	-	Ru	Ru	Ru	Gieklelite
SiO_2	40.6	40.7	41.0	41.2	42.2	42.5	38.1
Al_2O_3	13.6	14.1	13.8	13.9	12.7	12.2	16.7
TiO_2	2.1	2.3	2.4	1.3	8.6	6.2	5.0
MgO	27.3	26.7	26.5	28.1	20.7	22.7	24.0
K_2O	11.0	10.6	10.8	11.4	10.2	11.2	10.9
Sum	94.6	94.4	94.7	95.9	94.4	94.8	94.7
Si	5.730	5.732	5.769	5.733	5.908	5.958	5.375
Al	2.253	2.268	2.231	2.267	2.092	2.017	2.625
Al[1]	[0.017]	0.073	0.056	0.019	0.008	[0.025]	0.149
Ti	0.202	0.242	0.258	0.136	0.903	0.624	0.526
Mg	5.737	5.592	5.550	5.819	4.321	4.758	5.056
OSO	5.939	5.907	5.864	5.974	5.230	5.382	5.732
K	1.971	1.897	1.930	2.027	1.819	2.004	1.961
Ti-OSD	7.4	14.9	17.6	1.2	94.5	61.5	14.9
Ti-eastonite	13.0	10.1	9.0	12.4	4.7	1.1	23.8
Phlogopite	79.2	66.5	67.0	84.3	-	37.0	32.5
Eastonite[2]	[0.3]	8.5	6.5	2.2	0.7	[0.4]	14.9

Figure 2. Results of the experiments with the starting compositions A, B, C and D. Numbers indicate wt. % TiO_2 of the run product phlogopite (numbers in brackets indicate wt. % TiO_2 in the glass for two of the suprasolidus runs, comp. A), and symbols show the phase assemblage: single phase phlogopite (filled circles), melt + forsterite + phlogopite (open circles) and phlogopite + rutile (partly filled circles). Two of the experiments, marked (r), with composition B were isobarically reversed from 1150°C/20 kbar (6 hrs) to 1080°C/20 kbar (6 hrs) and from 1150°C/25 kbar (6 hrs) to 1100°C/25 kbar (6 hrs), respectively. The solubility limit of TiO_2 in phlogopite for composition B is indicated by a solid line, whereas the less well constrained solubility lines for the compositions A, C and D are dashed. The solidus of composition A is drawn as a dash-dot line.

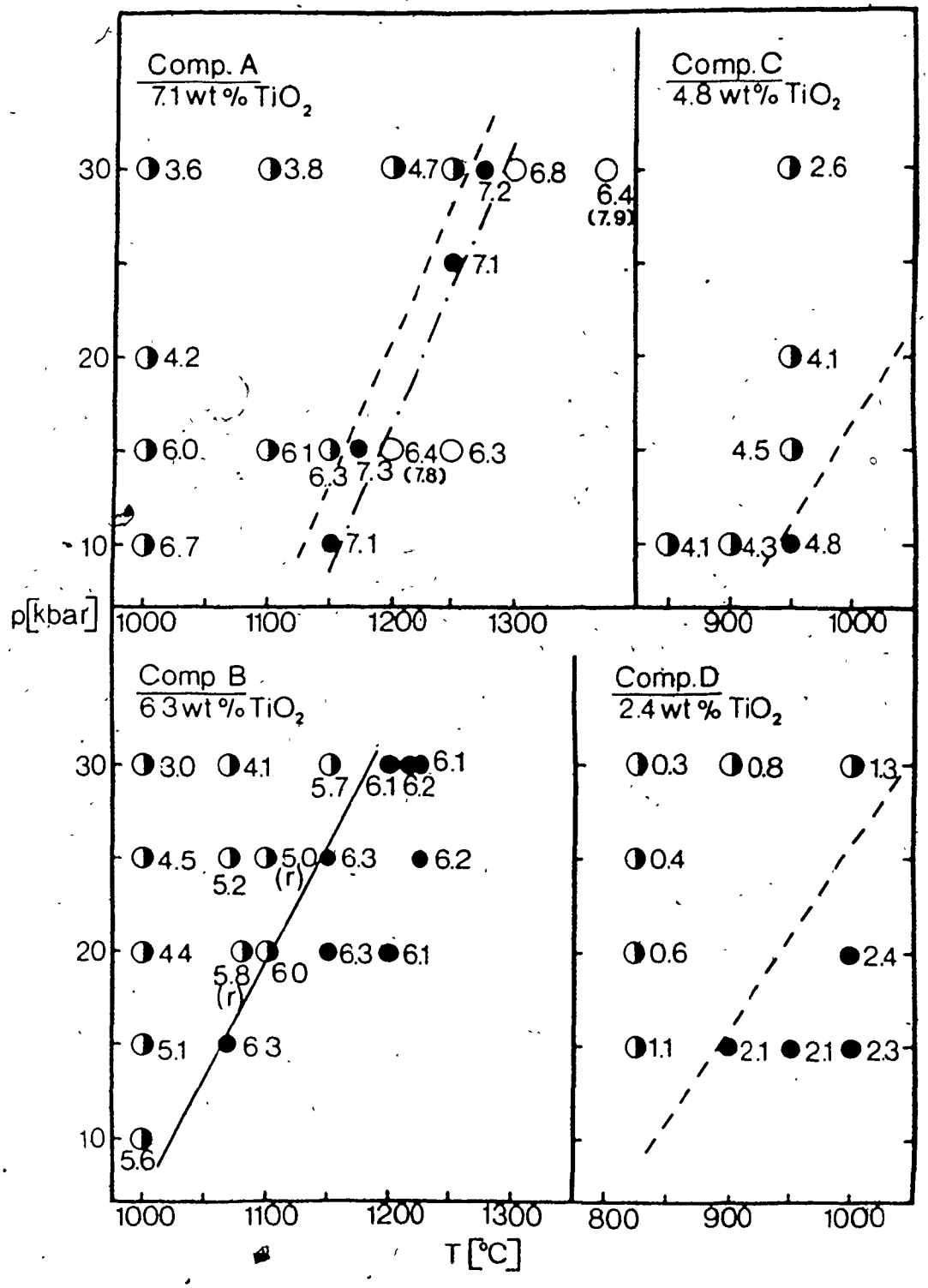
Comp. A
7.1 wt % TiO2
Comp. C
4.8 wt % TiO2
Comp B
6 3 wt % TiO2
Comp. D
2.4 wt % TiO2
p[kbar]
T [°C]
30
20
10
1000
1100
1200
1300
900
800
3.6
3.8
4.7
7.2
6.8
6.4
(7.9)
7.1
4.2
6.0
6.1
6.4
6.3
6.3
7.3
(7.8)
6.7
7.1
2.6
4.1
4.5
4.1
4.3
4.8
3.0
4.1
5.7
6.1
6.2
6.1
4.5
5.2
5.0
(r)
6.3
6.2
4.4
5.8
(r)
6.0
6.3
6.1
5.1
6 3
5.6
0.3
0.8
1.3
0.4
0.6
2.4
1.1
2.1
2.1
2.3

The solubility line separating the field of single phase phlogopite of composition close to the starting material from the field of phlogopite coexisting with rutile is most accurately located for the composition B (6.3 wt. % TiO_2). For the compositions A, C and D the solubility lines, representing the initial breakdown of a high-Ti phlogopite to form phlogopite + rutile as a function of decreasing temperature and increasing pressure, are less accurately constrained. At 10 kbar pressure the temperature of the solubility limit increases from about 840°C for the composition D (2.4 wt. % TiO_2), 940°C for composition C (4.8 wt. % TiO_2) and 1025°C for composition B (6.3 wt. % TiO_2) to about 1130°C for composition A (7.1 wt. % TiO_2). The four different solubility lines represent the saturation limit of TiO_2 in phlogopite for each of the starting material compositions, and none of them represent the maximum solubility of TiO_2 in phlogopite.

Four of the experiments at high temperatures on composition A resulted in run products containing glass coexisting with forsterite and minor phlogopite. Two glass analyses (15 kbar/1200°C and 30 kbar/1375°C) are included in Table 2. The solidus for composition A, located at about 1160°C at 10 kbar and 1300°C at 30 kbar, is lower than the solidi for the Ti-OSD end member (ca. 1330°C at 10 kbar) (Forbes & Flower, 1974) and for the phlogopite end member (ca. 1310°C at 10 kbar) (Yoder & Kushiro, 1969).

This indicates that a high-Ti phlogopite solid solution with a considerable proportion of the Ti-eastonite end member melts at a lower temperature than both the Ti-free phlogopite and the Ti-OSD end member.

Fig. 3 outlines the fields of single phase phlogopite, phlogopite + rutile and forsterite + phlogopite + melt. This temperature versus composition (along the join $K_2Mg_6Si_6Al_2O_{20}(OH)_4$-$K_2Mg_{4.5}TiSi_5Al_3O_{20}(OH)_4$) diagram contoured for pressure is based on the experimental results of this study and the solidus lines are interpolated in the directions towards the solidus temperatures of the Ti-free phlogopite composition ($K_2Mg_6Si_6Al_2O_{20}(OH)_4$) of Yoder & Kushiro (1969).

Figure 3. Temperature versus composition (along the join $K_2Mg_6Al_2Si_6O_{20}(OH)_4$-$K_2Mg_{4.5}TiAl_3Si_5O_{20}(OH)_4$) phase diagram contoured for pressure (10, 15, 20, 25 and 30 kbar). Open circles represent the near-solidus experiments (melt + forsterite + phlogopite) on composition A at 15 kbar and 30 kbar. The solidus lines are interpolated in the directions towards the solidus temperatures of the Ti-free phlogopite composition ($K_2Mg_6Al_2Si_6O_{20}(OH)_4$) of Yoder & Kushiro (1969).

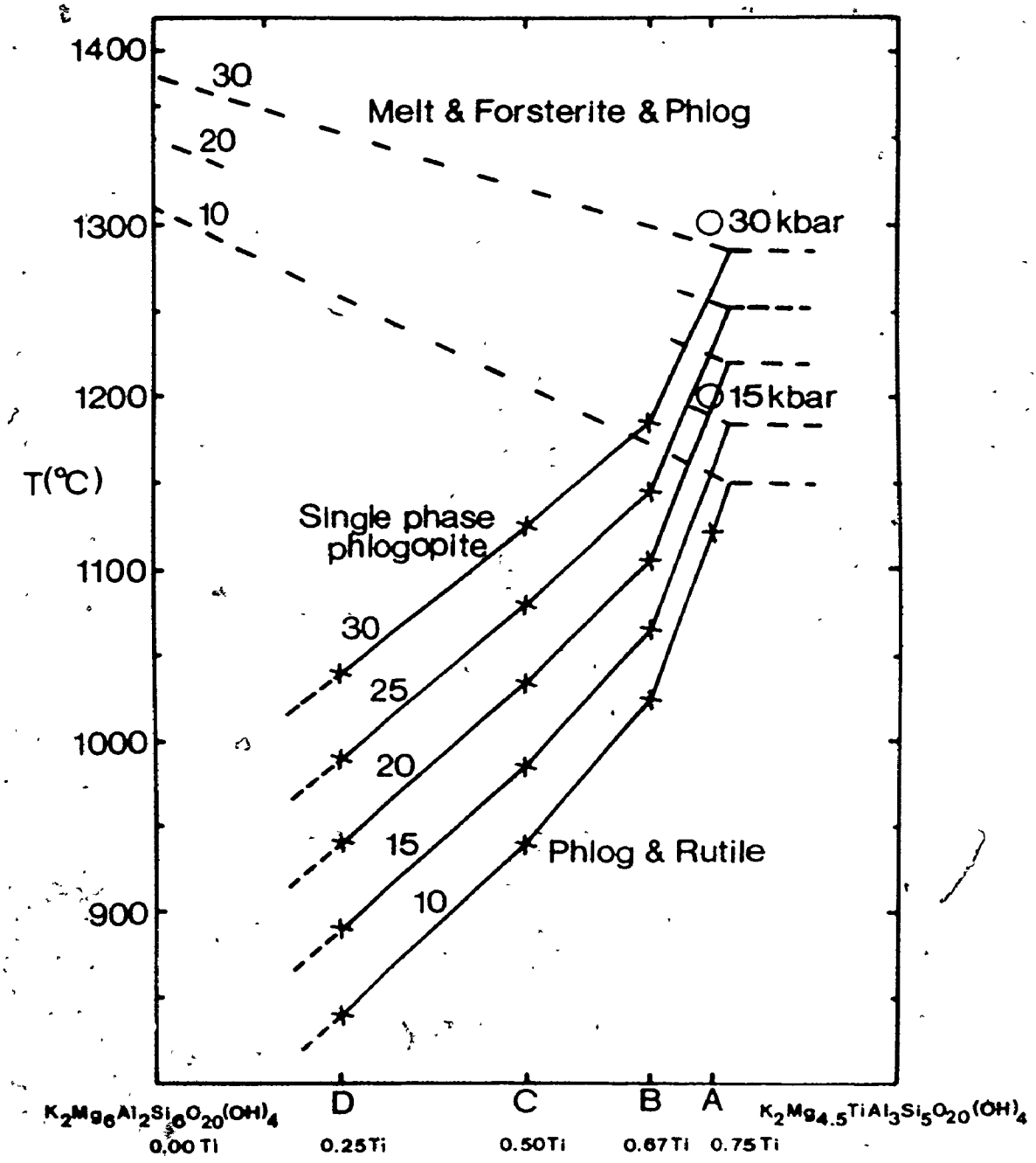
1400
1300
1200
1100
1000
900
T(°C)
30
20
10
Melt & Forsterite & Phlog
30 kbar
15 kbar
Single phase phlogopite
30
25
20
15
10
Phlog & Rutile
D
C
B
A
$K_2Mg_6Al_2Si_6O_{20}(OH)_4$
0.00 Ti
0.25 Ti
0.50 Ti
0.67 Ti
0.75 Ti
$K_2Mg_{4.5}TiAl_3Si_5O_{20}(OH)_4$

CHAPTER 4

COMPOSITIONAL RELATIONS OF PHLOGOPITES FROM THE EXPERIMENTAL STUDY AND NATURAL PHLOGOPITES

4.1 Structural formulae and simplified end member molecules

A number of cation substitutions control the compositions of the trioctahedral micas (see section 1.3). In order to study the incorporation of Ti in phlogopite, it was found advantageous to divide the phlogopite analyses into simplified end member molecules based on the structural formulae.

The procedures used for the calculation of the structural formulae are outlined in Appendix 4. A normalization to 22 oxygen anions (charge of 44) has been used. Since the trioctahedral micas have considerable variations in the number of cations per unit cell (Deer et al., 1965;

Green, 1982; Dymek, 1983), a normalization to a given number of cations (e.g. 6 octahedral + 8 tetrahedral) per unit cell will normally result in a charge that differs significantly from the ideal value of 44.

The calculation of the end member molecules from the structural formulae is designed to illustrate the mechanisms of Ti-incorporation in phlogopite, and to provide a basis of comparison of the phlogopites of natural compositions with those produced experimentally from synthetic starting materials. The principles of the applied calculation procedure are to separate the Ti-free components from the Ti-OSD and the Ti-eastonite end member molecules. The calculation procedure, which maintains stoichiometry and charge balance for all of the end member molecules, is outlined in Appendix 4. By using this procedure the simplified phlogopite compositions from the experiments are divided into the following molecules.

1. Ti-OSD end member, $K_2(Mg_4Ti)(Si_6Al_2)O_{20}(OH)_4$
2. Ti-eastonite end member, $K_2(Mg_5Ti)(Si_4Al_4)O_{20}(OH)_4$
3. Phlogopite end member, $K_2Mg_6(Si_6Al_2)O_{20}(OH)_4$
4. Eastonite end member, $K_2(Mg_5Al)(Si_5Al_3)O_{20}(OH)_4$

The phlogopites of natural compositions are also separated into the same end members 1-3, whereas the eastonite molecule will in some cases include Cr in addition to Al (Appendix 4).

4.2 Chemistry of experimentally produced phlogopites of synthetic composition

The compositions and structural formulae of the phlogopites produced during the experimental study are given in Table 2, which also lists the proportions of the 4 end member molecules for these phlogopites. In Fig. 4 Ti is plotted against the parameter (6-OSO) + $(6\text{-Si-Al}^{VI})/2$. The octahedral site deficiency (6-OSO, where OSO = octahedral site occupancy) is a measure of the substitution $2Mg = Ti\square$, whereas the parameter $(6\text{-Si-Al}^{VI})/2$ expresses the substitution $Mg(2Si) = Ti(2Al)$. The phlogopite compositions are confined to a narrow band just above the line through the origin and with a slope of unity. This indicates that essentially all of the Ti has been incorporated by a combination of the two substitution mechanisms represented by the end member molecules Ti-OSD and Ti-eastonite.

The most likely explanation for the very minor, but consistent displacement of the points upwards from the unity line ($Ti > [6\text{-OSO} + (6\text{-Si-Al}^{VI})/2]$) is that a minor part of the octahedral site deficiency is caused by Al^{VI}. Much more pronounced trends towards dioctahedral mica (i.e. muscovite type substitution) in phlogopites crystallized under high pressure conditions were observed by Green (1982) and Chopin (1984).

Fig. 5a and b show that the experimentally produced

Figure 4. The Ti vs. 6-OSO + 1/2(6-Si-Al^{VI}) relationship for the experimentally produced phlogopites (OSO: octahedral site occupancy). The large, open symbols with an internal cross represent ideal starting composition phlogopites. Composition A: dots (open circle for starting composition), comp. B: diamonds, comp. C: squares, comp. D: triangles.

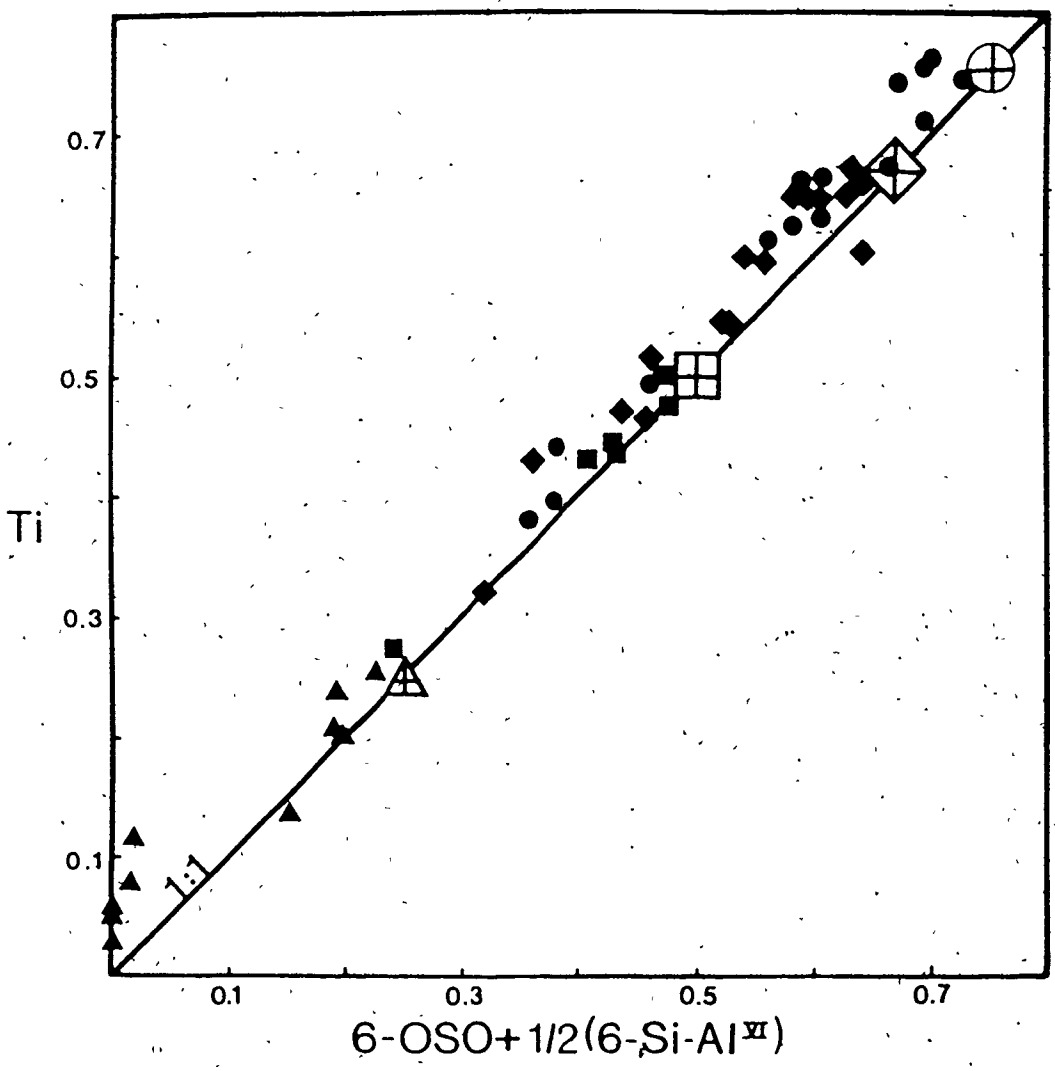
0.7
0.5
0.3
0.1
Ti
1:1
0.1
0.3
0.5
0.7
6-OSO+1/2(6-Si-Al^VI)

Figure 5a. Ti vs. Al^{VI} for the experimentally produced phlogopites. Symbols as in Fig. 4.

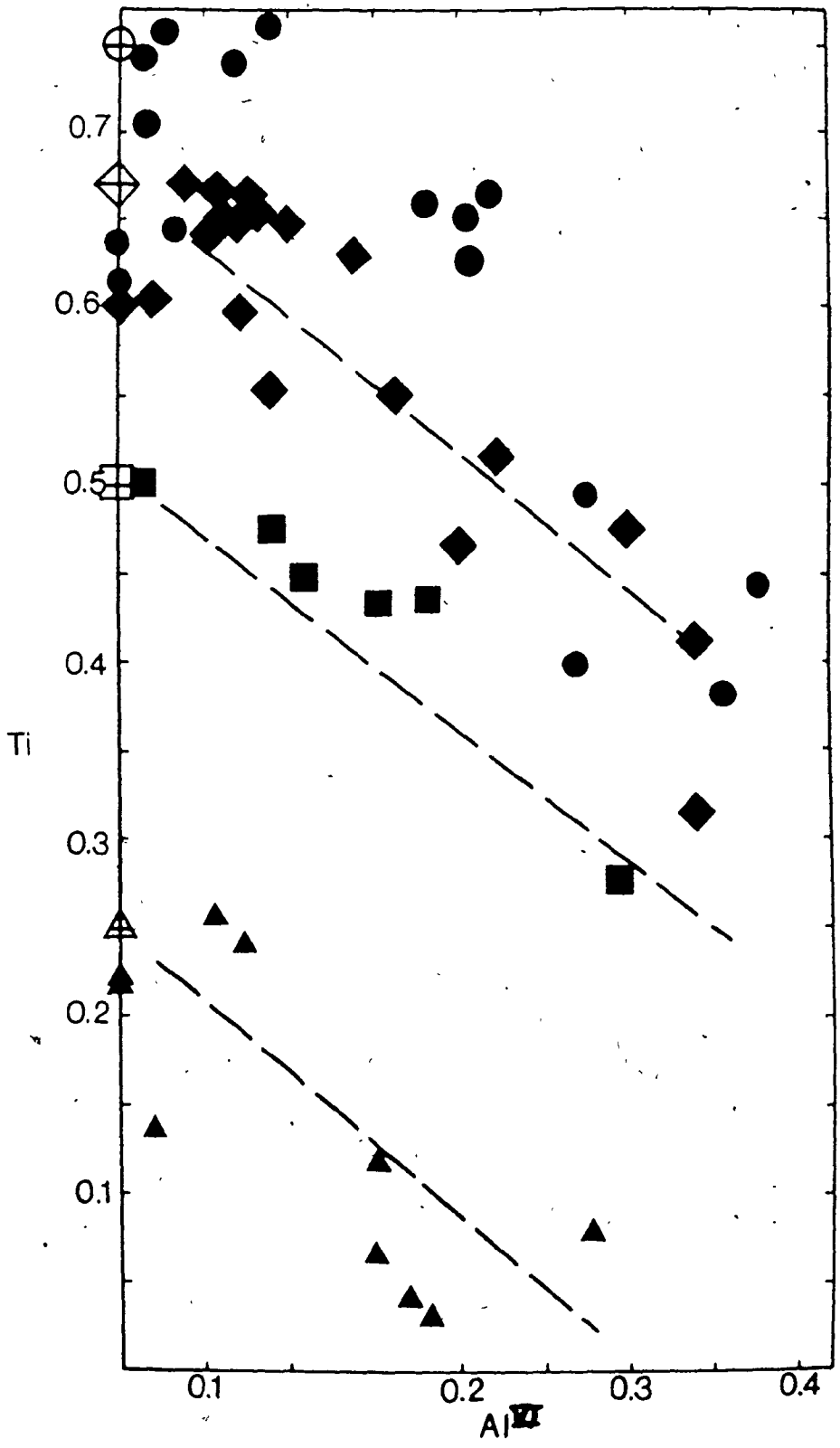
0.7
0.6
0.5
0.4
Ti
0.3
0.2
0.1
0.1
0.2
0.3
0.4
Al[VI]

Figure 5b. Ti vs. Al^{VI} for the experimentally produced phlogopites along three isothermal sections (1000°C for compositions A and B and 950°C for composition C). Symbols as in Fig. 4.

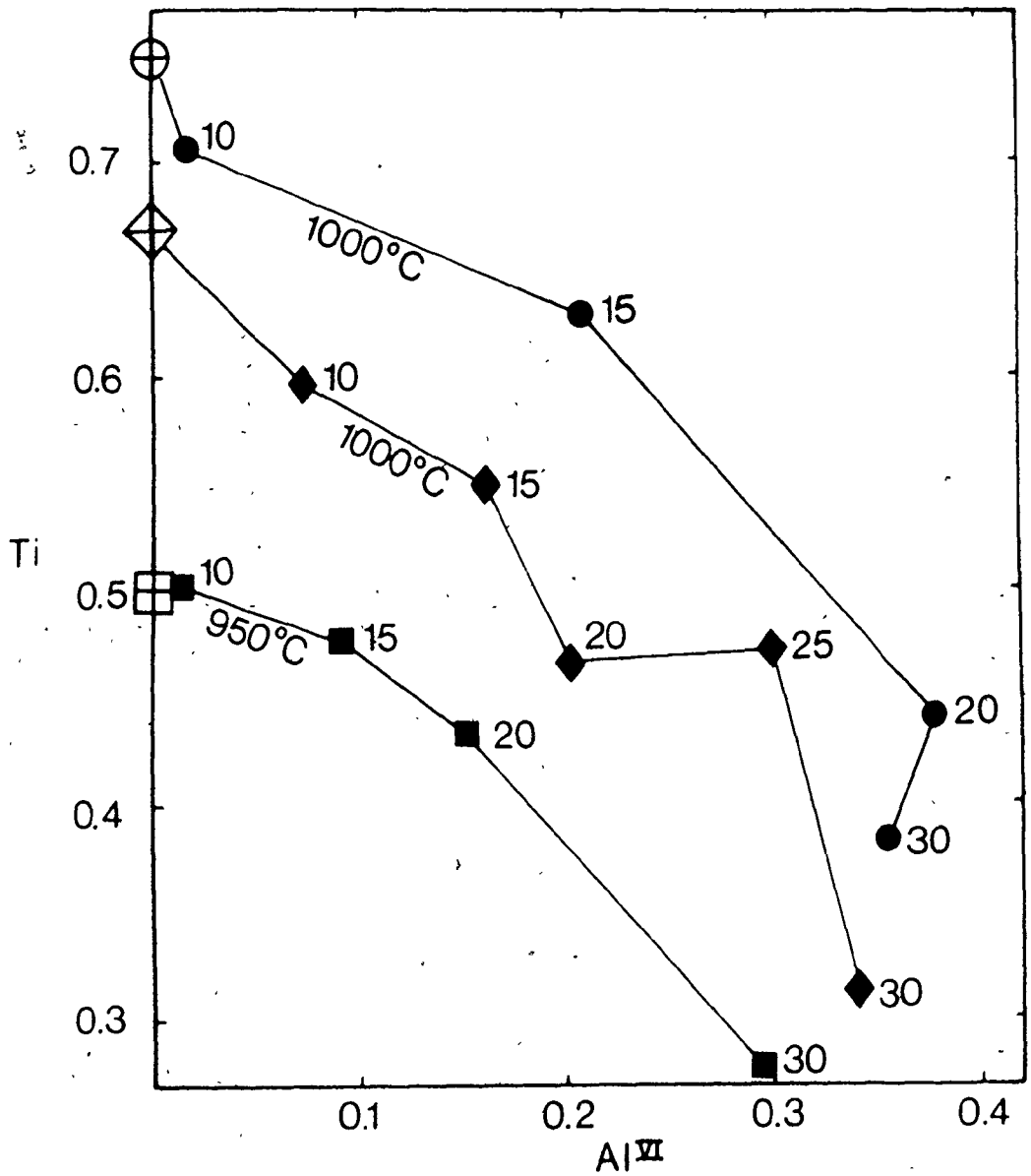
0.7
0.6
0.5
0.4
0.3
Ti
0.1
0.2
0.3
0.4
AlVI
10
1000°C
15
10
1000°C
15
10
950°C
15
20
20
25
20
30
30
30

Figure 6. The Ti-OSD molecule and the Ti-eastonite molecule as a function of Al^{VI} and the eastonite molecule for the same isothermal sections as those in Fig. 5b. The scales for the end member molecules are number of tetrahedral cations per formula unit (O = 22, sum tetrahedral cations = 8). Symbols as in Fig. 4.

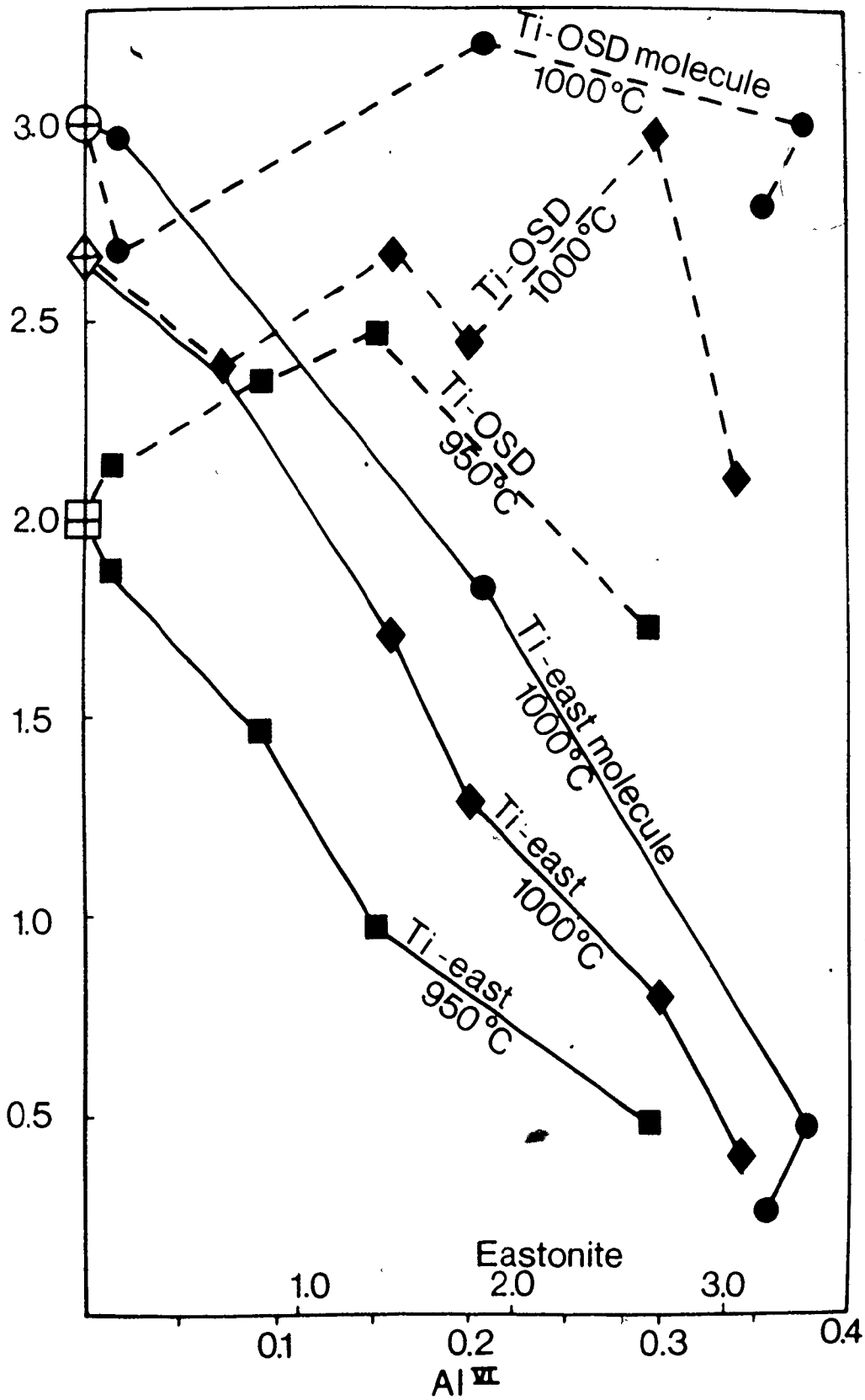
Ti-OSD molecule
1000°C
Ti-OSD
1000°C
Ti-OSD
950°C
Ti-east molecule
1000°C
Ti-east
1000°C
Ti-east
950°C
3.0
2.5
2.0
1.5
1.0
0.5
Eastonite
1.0
2.0
3.0
0.1
0.2
0.3
0.4
AlVI

Figure 7. Compositional relations between the end member molecules (molecular percent) Ti-OSD, Ti-eastonite and phlogopite + eastonite for the experimentally produced phlogopites. The starting compositions A, B, C and D are shown as open circles with internal crosses. The other symbols as in Fig. 2. The lower right diagram shows the composition of the phlogopites produced in runs with the Ti-OSD and the Ti-eastonite end members as starting materials.

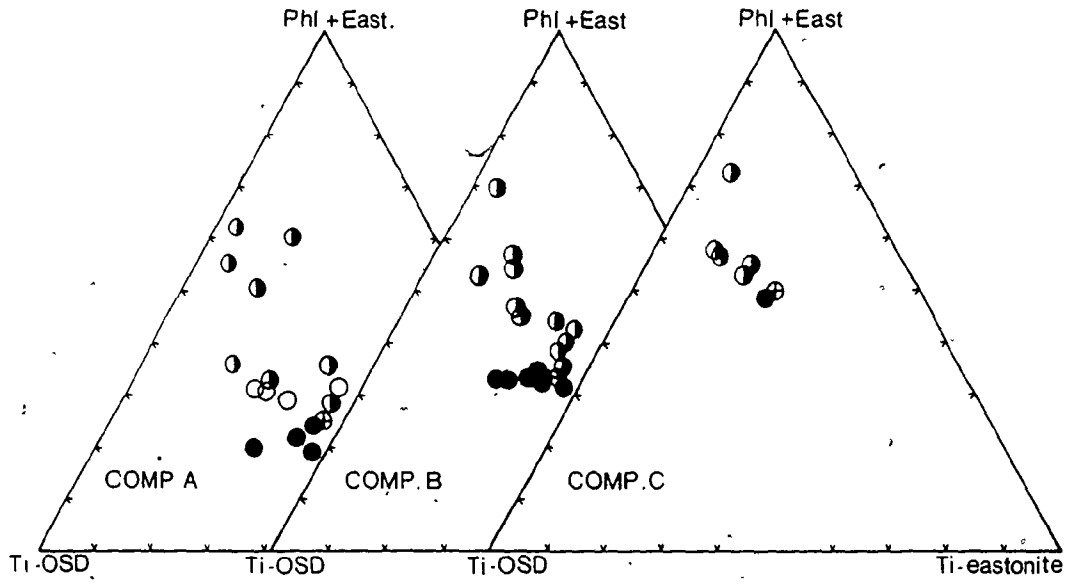
Phl +East.
Phl +East
Phl +East
COMP A
COMP. B
COMP.C
Ti-OSD
Ti-OSD
Ti-OSD
Ti-eastonite

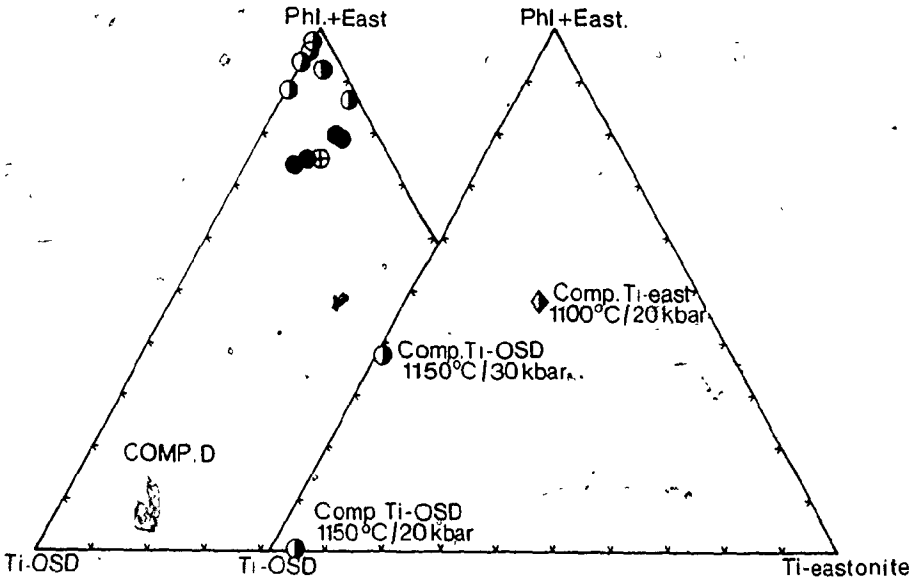
Phl.+East
Phl+East.
Comp. Ti-east
1100°C/20kbar
Comp.Ti-OSD
1150°C/30kbar
COMP.D
Comp Ti-OSD
1150°C/20kbar
Ti-OSD
Ti-OSD
Ti-eastonite

phlogopites are characterized by a negative correlation between Ti and Al^{VI}. This relationship is linked to the negative correlation between the eastonite end member (Al^{VI}) and the Ti-eastonite end member (Fig. 6). Fig. 6 also shows that the variation in the amount of the Ti-OSD molecule is much less regular. However, a minor decrease in the amount of this end member seems to be associated with increasing amount of eastonite and decreasing amount of total Ti (Fig. 5 and 6).

Fig. 7 shows the compositional relations between the end members Ti-OSD, Ti-eastonite, and the sum phlogopite + eastonite. The corner phlogopite + eastonite represents the Ti-free part of the phlogopite solid solution. When a high-Ti phlogopite solid solution containing equal proportions of the Ti-OSD and Ti-eastonite molecules breaks down to a low-Ti phlogopite solid solution coexisting with rutile, the ratios Ti-eastonite/Ti-OSD and phlogopite/eastonite both decrease (Table 2, Fig. 5-7).

4.3 Chemistry of natural phlogopites

A survey of published phlogopite analyses was carried out in order to evaluate the chemistry of phlogopites of natural compositions that crystallized under conditions comparable to those of the experimental study. About 700 analyses were selected from reports of:

1. Mantle fragments in kimberlites and alkaline

volcanics.

2. High-pressure megacrysts and cumulate inclusions in kimberlites and alkaline volcanics.
3. Phenocrysts and groundmass in kimberlites and alkaline volcanic and subvolcanic.
4. Melting experiments on ultrapotassic rock compositions.
5. Granulite facies metamorphic rocks.

Appendix 5 lists the sources of these analyses. Analyses with an atomic ratio Mg/(Mg + Fe) of less than 0.667 (the phlogopite-biotite division line suggested by Deer et al., 1965) were excluded from the data collection.

A separation has been made between the mineral assemblages that include a Ti-rich oxide phase (rutile, ilmenite or perovskite) and those without such a phase.

The phlogopites are almost invariably characterized by an octahedral site deficiency (6- octahedral cations). The average deficiency number is about 0.2 per formula unit. This is a characteristic feature of the trioctahedral micas (Deer et al., 1965), and it is almost certainly caused mainly by substitutions of 3- and 4-valency cations in the octahedral sites (Arima & Edgar, 1981; Green, 1982; Dymek, 1983). Most of the phlogopites have also a deficiency of 12-coordinated interlayer cations. The average sum of K, Na, Ca and Ba is about 1.92 per formula unit. This deficiency may largely be a result of preferential volatil-

ization of Na and K during microprobe analyses. No correlation was found between the interlayer deficiency and the amount of divalent interlayer cations (Ca and Ba), so it is unlikely that the deficiency is caused by the theoretical substitution $2(K,Na) = (Ca,Ba) + \square$ (section 1.3).

In Fig. 8a the phlogopite compositions with Si+Al+Cr $\geq$ 8 are plotted as Ti against the parameter $6\text{-}OSO + (6\text{-}Si\text{-}Al^{VI}\text{-}Cr^{VI}\text{-}Ca\text{-}Ba)/2$, and Fig. 8b shows Ti versus $6\text{-}OSO+(6\text{-}Si\text{-}Ca\text{-}Ba)/2$ for the analyses with Si+Al+Cr < 8. These figures correspond to Fig. 4 for the simplified, synthetic phlogopite compositions, and the terms including Al^{VI}, Cr^{VI}, Ca and Ba represent the corrections for the influence of the substitutions $Mg^{VI}Si^{IV} = (Al,Cr)^{VI}(Al,Cr)^{IV}$ and $K^{XII}Si^{IV} = (Ca,Ba)^{XII}Al^{IV}$. The natural phlogopite compositions are comparable to the simplified, synthetic compositions in the sense that they cluster in a narrow band along, but slightly above the line through the origin and with a slope of unity. The phlogopites with Si+Al+Cr $\geq$ 8 plot more consistently above the 1:1 relation line than the phlogopites with Si+Al+Cr < 8. This confirms that Ti is incorporated mainly by the substitutions $2Mg = Ti\square$ and $Mg^{VI}(2Si)^{IV} = Ti^{VI}(2Al)^{IV}$, even in the phlogopites with Si+Al+Cr < 8. The minor displacement of the compositions upwards from the line may be caused by a substi-

Figure 8a. The Ti vs. 6-OSO + 1/2(6-Si-Al^{VI}-Cr^{VI}-Ca-Ba) for the natural phlogopites with Si+Al+Cr $\geq$ 8. The data sources are listed in Appendix 5.

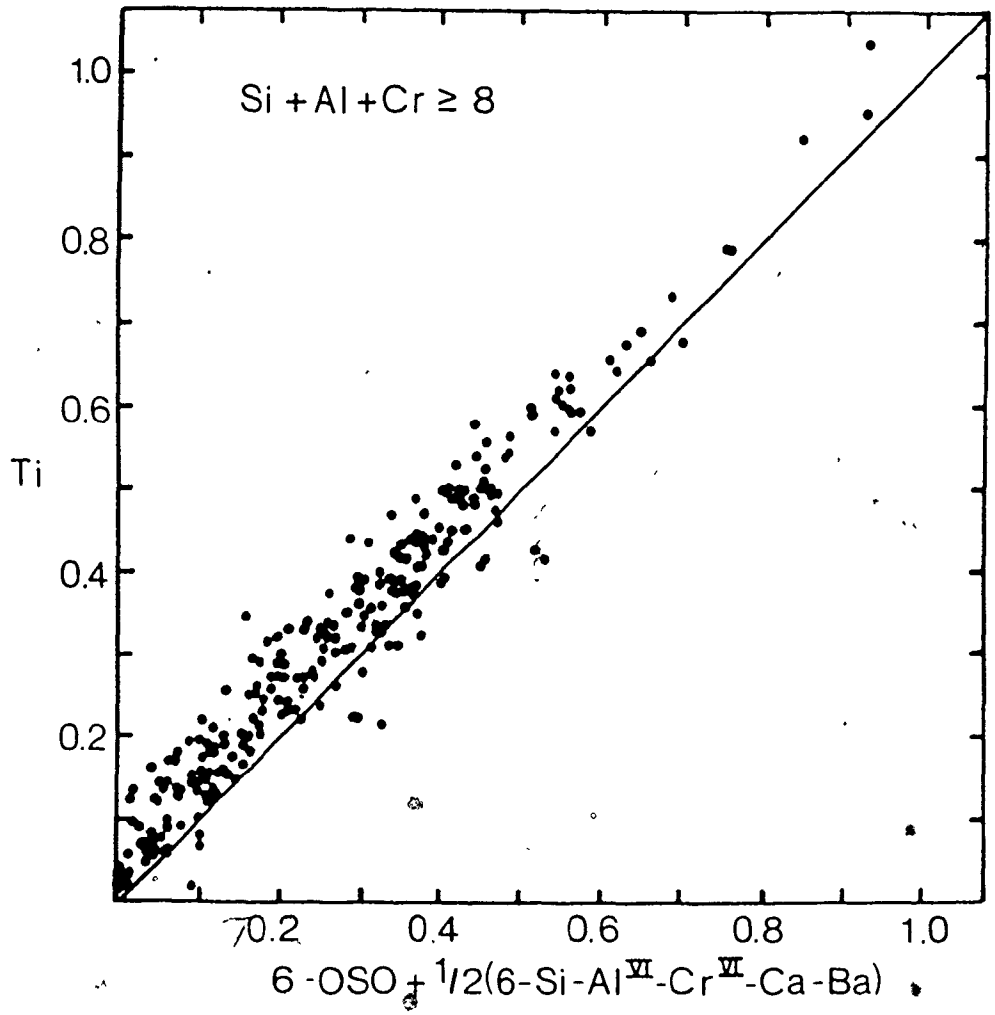
Si + Al + Cr ≥ 8
Ti
1.0
0.8
0.6
0.4
0.2
0.2
0.4
0.6
0.8
1.0
6 - OSO + 1/2(6 - Si - Al^VI - Cr^VI - Ca - Ba)

Figure 8b. The Ti vs. 6-OSO + 1/2(6-Si-Ca-Ba) relationship for the natural phlogopites with Si+Al+Cr < 8 ($Si+Al+Cr+Fe^{3+}_{calculated} = 8$). The phlogopite analyses from the Shaw's Cove minette (Bachinski & Simpson, 1984) fall off the main trend and are indicated by open circles. The data sources are listed in Appendix 5.

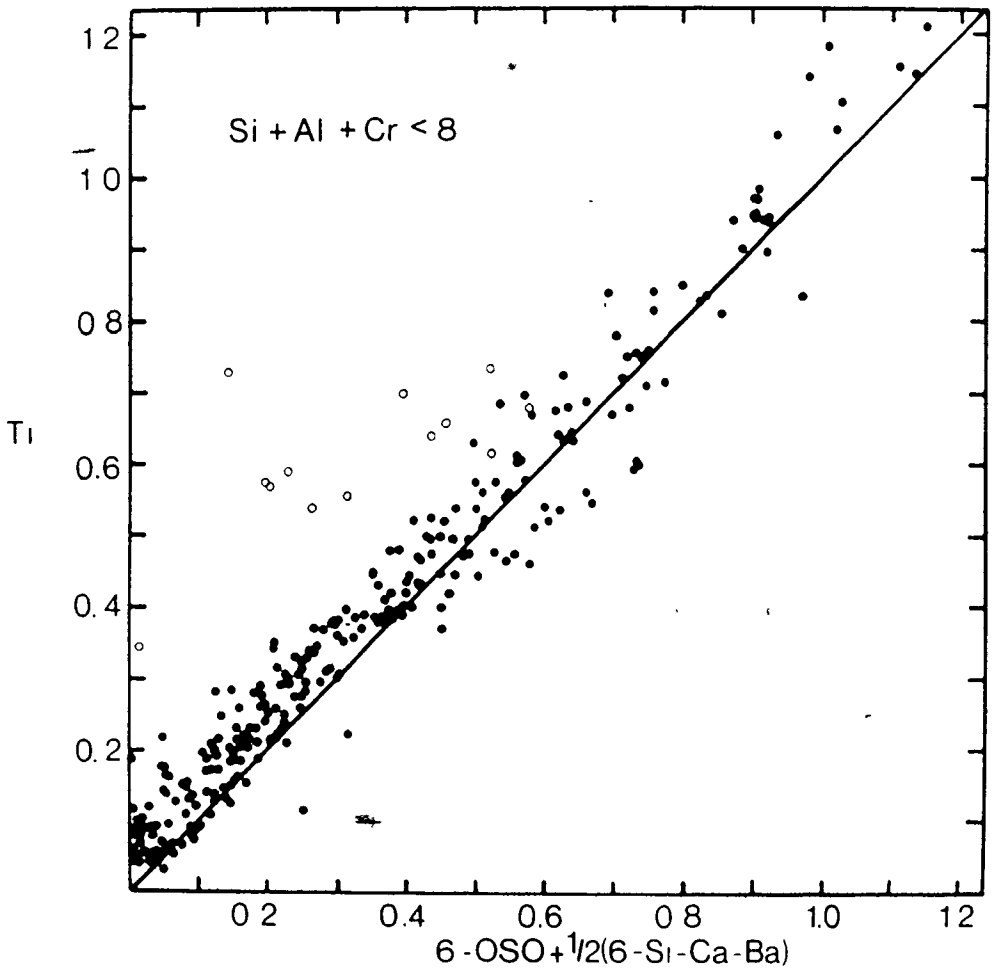
Si + Al + Cr < 8
Ti
1.2
1.0
0.8
0.6
0.4
0.2
0.2
0.4
0.6
0.8
1.0
1.2
6 - OSO + 1/2(6 - Si - Ca - Ba)

tutional relationship of a small part of the octahedral site deficiency with some of the octahedral Al and Cr and possibly with some of the interlayer Ba and Ca.

Most of the phlogopites from the Shaw's Cove minette (Bachinski & Simpson, 1984) with an excess of OSO cations fall markedly outside the trend (Ti > (6-Si-Ca-Ba)/2). Bachinski & Simpson (1984) suggest that some of the OSO cations are located in the interlayer sites to compensate for large deficiencies of interlayer site cations and high Al/Si ratios.

In Fig. 9 to 12 a representative selection of natural phlogopite compositions are displayed in the triangular diagram showing the relative proportions of the Ti-OSD and Ti-eastonite end member molecules and the sum of the Ti-free molecules. The tendency to displacement of the compositions towards the Ti-OSD - sum of Ti-free molecules join is in accordance with the phlogopite compositions of the experimental run products.

The majority of the phlogopite compositions shown in Fig. 9-12 have $Si+Al+Cr \geq 8$, and the amount of eastonite varies from zero to about 40 mol. % in these phlogopites. About one half of the total number of selected phlogopite analyses have $Si+Al+Cr < 8$ ($Si+Al+Cr+Fe^{3+} = 8$), where the value of Fe^{3+} is calculated, Appendix 4). The average eastonite content of the naturally occurring phlogopites is therefore lower (about 3%), but the ranges of eastonite contents exceed those of the experimentally produced

Figure 9. Compositional relations between the end members Ti-OSD, Ti-eastonite and the sum of the Ti-free molecules for phlogopites in mantle xenoliths in kimberlites and alkaline volcanics.

a. Dots: Garnet lherzolites in Namibian kimberlites (Mitchell, 1984); squares: peridotites and pyroxenites from Bullenmerri and Gnotuk maars, Victoria, Australia (Griffin et al., 1984); diamonds: peridotites in the Bultfontein kimberlite, South Africa (Jones et al., 1982).

b. Open circles with crosses: primary textured phlogopites secondary textured phlogopites in mantle xenoliths (Delaney et al., 1980); squares: alkali pyroxenites in ankaramitic scoria and carbonatitic tuff, Lashaine volcano, Tanzania (Dawson & Smith, 1972); diamonds: lherzolites in basanoids, Ubekendt Ejland, Greenland (Larsen, 1982).

c. Open circles with crosses: primary textured phlogopites and dots: secondary textured phlogopites in lherzolite xenoliths (Carswell, 1975); squares: garnet lherzolites and megacrystalline nodules in potassic lamprophyres, Navajo Volcanic Field, USA (Ehrenberg, 1982); diamonds: ultramafic xenoliths in basanites, Victoria, Australia (Nickel & Green, 1984).

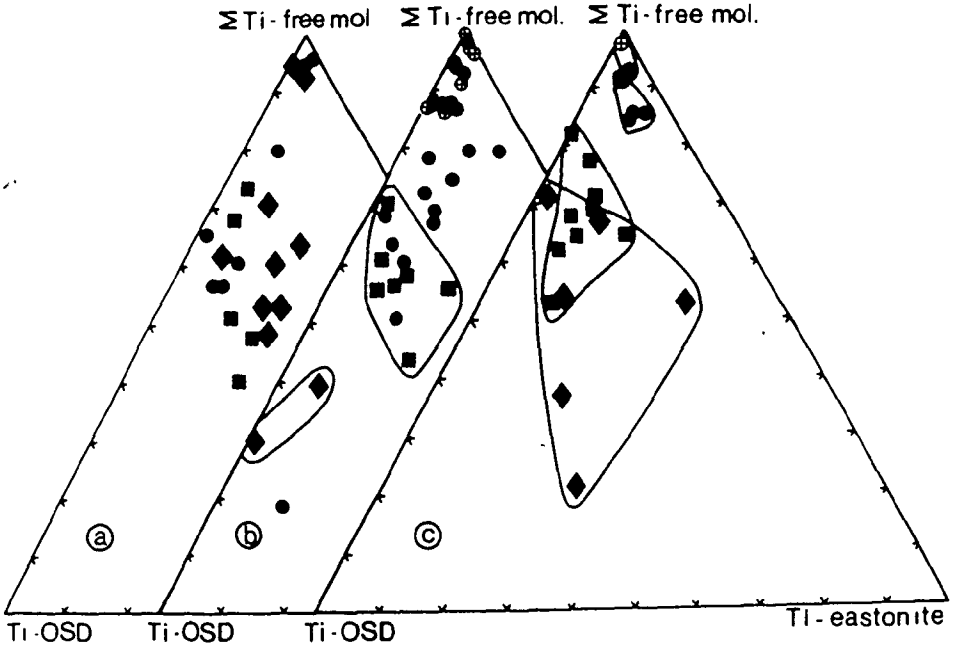
Σ Ti - free mol
Σ Ti - free mol.
Σ Ti - free mol.
ⓐ
ⓑ
ⓒ
Ti-OSD
Ti-OSD
Ti-OSD
Ti - eastonite

Figure 10. Compositions of phlogopites in kimberlites and lamprophyres.

a. Dots: groundmass phlogopite in kimberlites from South Africa and Canada (Sm[redacted] et al., 1978); squares: phenocrysts in the Jos Dyke kimberlite, N.W.T., Canada (Mitchell & Meyer, 1980); diamonds: high pressure megacrysts in the Fayette County kimberlite, Pennsylvania, USA (Hunter & Taylor, 1984).

b. Dots: groundmass phlogopite in the Pendennis peralkaline minette, Cornwall, England (Hall, 1982); squares: phenocrysts in the Tunraq kimberlite, N.W.T., Canada (Mitchell, 1979); diamonds: phenocrysts in basanites and tephrites, Laacher Sea, West Germany (Duda & Schminke, 1978); triangles: groundmass and phenocrysts in kimberlites and lamprophyres, Holsteinborg, West Greenland (Scott, 1979).

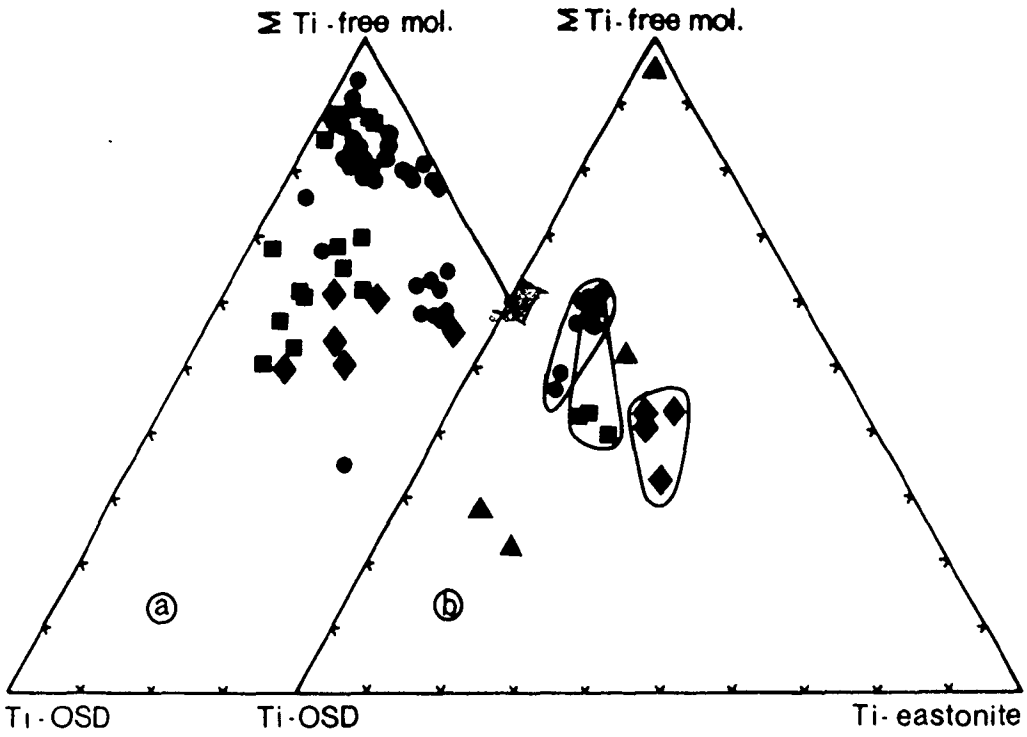
Σ Ti - free mol.
Σ Ti - free mol.
ⓐ
ⓑ
Ti - OSD
Ti - OSD
Ti - eastonite

Figure 11. Compositions of phlogopites from K-rich mafic and ultramafic volcanic and subvolcanic rocks.

a. Dots: phenocryst (P) and groundmass (G) phlogopites in ultrapotassic rocks, Sierra Nevada, USA (Van Kooten, 1980); squares: megacrysts and cognate inclusions in alkali basalt, West Eifel, West Germany (Aoki & Kushiro, 1968); diamond: high pressure cognate inclusions in basanite, hawaiite and mugearite, Victoria, Australia (Ellis, 1976); triangle: high pressure cognate inclusions in lava and tuff of alkali olivine basalt composition, Arizona, USA (Evans & Nash, 1979).

b. Dots: phenocryst cores (C) and phenocryst rims, groundmass and resorbed phenocrysts (R) in lamproites, West Kimberley, Western Australia (Mitchell, 1981); squares: phenocryst cores and diamonds: groundmass and phenocryst rims, Shaw's Cove minette, New Brunswick, Canada (Bachinski & Simpson, 1984); triangle: average composition of phlogopites in minettes (Bachinski & Simpson, 1984).

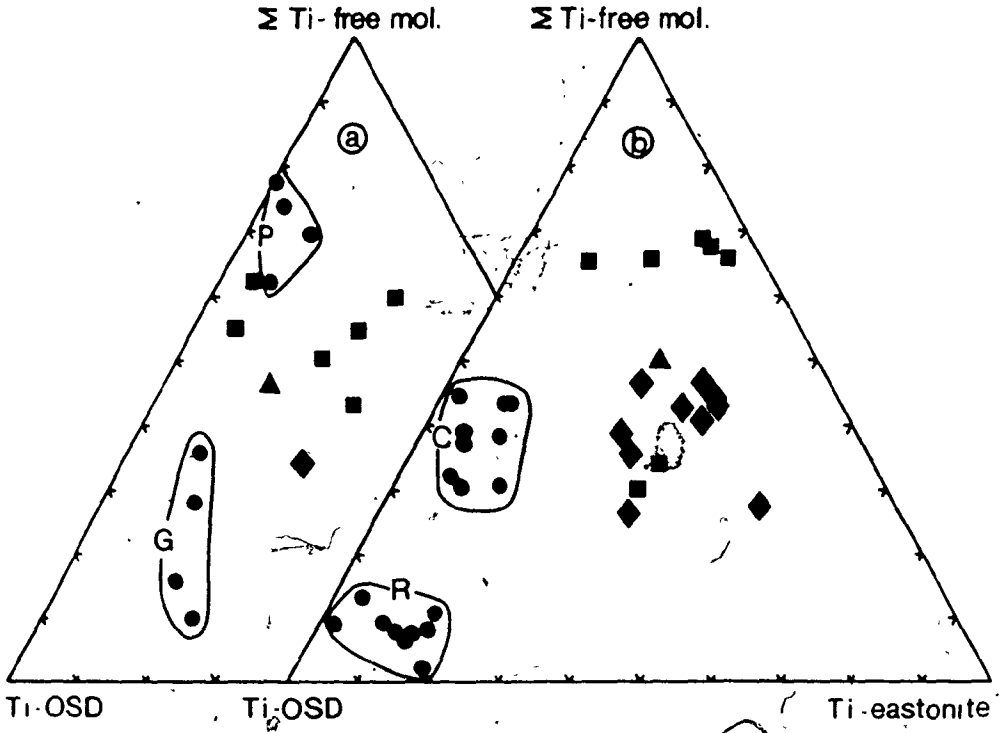
Σ Ti- free mol.
Σ Ti-free mol.
ⓐ
ⓑ
P
G
C
R
Ti-OSD
Ti-OSD
Ti-eastonite

Figure 12. Compositions of phlogopites crystallized during melting experiments with ultrapotassic rock compositions (a) and phlogopites from granulite facies metamorphic rocks (b and c).

a. Melting experiments with: dots: biotite mafurite (Edgar et al., 1976); squares: katungite (Arima & Edgar, 1983); diamonds: wolgidite (Arima & Edgar, 1983).

b. Dots: metapelitic orthopyroxene gneisses and squares: mafic pyribolitic granulites, Godthab District, West Greenland (Dymek, 1983).

c. Dots: sapphirine bearing feldspar-sillimanite gneisses, Pikwitonei, Manitoba, Canada (Arima & Barnett, 1984); squares: sapphirine-quartz-sillimanite-orthopyroxene granulites, Enderby Land, Antarctica (Grew, 1980); diamonds: orthopyroxene-cordierite gneisses and triangles: two-pyroxene gneisses, Namaqualand, South Africa (Clifford et al., 1981).

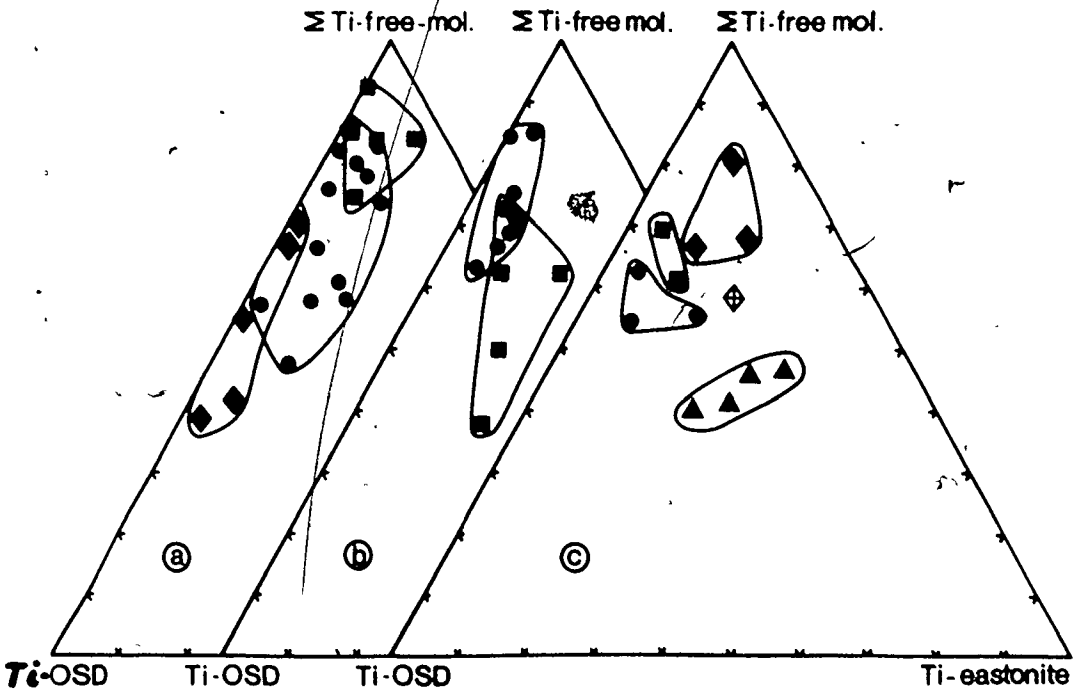
Σ Ti-free-mol.
Σ Ti-free mol.
Σ Ti-free mol.
ⓐ
ⓑ
ⓒ
Ti-OSD
Ti-OSD
Ti-OSD
Ti-eastonite

synthetic phlogopites.

About half of the phlogopites in the mantle xenoliths coexist with a Ti-rich oxide phase (rutile, ilmenite or perovskite), and about one third of the phlogopites that crystallized from a melt under high pressure (including the experimentally crystallized ultrapotassic rock samples) coprecipitated with a Ti-rich oxide mineral. Almost all of the phlogopites in granulites coexist with such a phase. However, no clear relationship between the phlogopite composition and the presence or absence of rutile, ilmenite and perovskite has been found.

4.4 Crystal chemical relations for the end member molecules

The cation substitutions in the trioctahedral mica group have profound effects on crystal structure, physical properties and stability (Radoslovich and Norrish, 1962; Hazen and Wones, 1972). The composition of phlogopite is partly governed by the charge balance requirement, but this is not the only limiting factor to compositional variation. Crystal chemical relationships and their bearing on the crystal structure may explain the relative stability, and therefore the relative abundances, of the Ti-rich and the Ti-free end member molecules in phlogopite solid solutions.

As pointed out by Radoslovich and Norrish (1962)

structural misfits exist between the $AlSi_3$ tetrahedral layer and the smaller Mg_3 octahedral layer in phlogopite, and between the $AlSi_3$ tetrahedral layer and the larger Fe_3 octahedral layer in annite. Hazen and Wones (1972) demonstrated linear relationships between the average ionic radius of the cations present and the unit cell dimensions, especially the a and b dimensions. The cation-oxygen framework of the tetrahedral and octahedral layers must coincide, either by an appropriate combination of cations or by bond angle modification, if the mica structure is to be stable (Radoslovich and Norrish, 1962; Hazen and Wones, 1972).

Although the structural misfit between the larger tetrahedral and the smaller octahedral layers in the phlogopite end member can be reduced to zero by bond angle modification, such a reduction may be impossible in the eastonite molecule. The coupled substitution of Al in both the tetrahedral and the octahedral sites to form eastonite will increase the structural discrepancy considerably (Al^{IV} has larger radius than Si^{IV}, and Al^{VI} has smaller radius than Mg^{VI}). The crystallostructural misfit between the tetrahedral and octahedral layers becomes even greater in the Ti-eastonite molecule with a higher proportion of tetrahedral Al combined with the octahedral substitution of Ti for Mg.

The Ti-OSD end member, however, has probably a smaller

misfit between the octahedral and tetrahedral layers than those of both eastonite and Ti-eastonite, since the tetrahedral site composition of the Ti-OSD molecule is identical to that of the phlogopite molecule. This may explain why the incorporation of Ti in phlogopite is primarily in the form of the Ti-OSD end member rather than the Ti-eastonite end member.

With increasing pressure silicate minerals with high proportions of Al^{IV} are generally replaced by denser minerals with lower Al^{IV}-contents and higher Al^{VI}/Al^{IV} ratios (e.g. Chopin and Maresch, 1984). This is in accordance with the decreasing proportion of the Ti-eastonite molecule ($Al^{IV}/Si^{IV} = 1$, $Al^{VI}/Al^{IV} = 0$) and the increasing proportion of the eastonite molecule ($Al^{IV}/Si^{IV} = 3/5$, $Al^{VI}/Al^{IV} = 1/3$) in the phlogopite solid solution as the pressure increases. The proportions of the Ti-OSD and the phlogopite end members (both with $Al^{IV}/Si^{IV} = 1/3$ and $Al^{VI}/Al^{IV} = 0$) appear to be relatively unaffected by the pressure.

CHAPTER 5

GEOTHERMOMETRY AND GEOBAROMETRY

5.1 The experimentally derived phlogopite geothermobarometer

The relations between temperature, pressure and Ti-content of phlogopite documented by the experimental study suggest that the Ti-content of natural phlogopites may represent a potential geothermobarometer. Other studies have also indicated such a potential (e.g. Arima & Edgar, 1981; Ghent & Stout, 1984; Guidotti, 1984; Hewitt & Wones, 1984; Otten, 1984).

The phlogopite geothermobarometer developed for the assessment of this potential is based on the Ti-OSD - Ti-eastonite-ΣTi-free components triangular diagram. Isobaric diagrams with contours for temperature (Fig. 13) and isothermal diagrams with pressure contours (Fig. 14)

Figure 13a. Isobaric compositional diagrams (7.5, 10, 15 and 20 kbar) contoured for temperature based on the experimental data. The phlogopite compositions from rocks with independent temperature and pressure determinations are plotted on the diagrams:

Dots: garnet lherzolites in Namibian kimberlites, the sample number is given for each composition (Mitchell, 1984); squares: ultramafic xenoliths from Bullenmerri and Gnotuk maars, Victoria, Australia, with sample numbers (Griffin et al., 1984). For the rest of the localities the compositional range is outlined. 1: orthopyroxene gneisses and 2: mafic pyribolitic granulites, Godthab District, West Greenland (Dymek, 1983); 3: sapphirine-quartz-sillimanite-orthopyroxene granulites, Enderby Land, Antarctica (Grew, 1980); 4: sapphirine bearing feldspar-sillimanite gneisses, Pikwitonei, Manitoba, Canada (Arima & Barnett, 1984); 5: lherzolites in basanites, Victoria, Australia (Nickel & Green, 1984); 6: garnet lherzolites in lamprophyres, Navajo Volcanic Field, USA (Ehrenberg, 1982); 7: garnet lherzolites in kimberlite, Premier Mine, South Africa (Danchin, 1979).

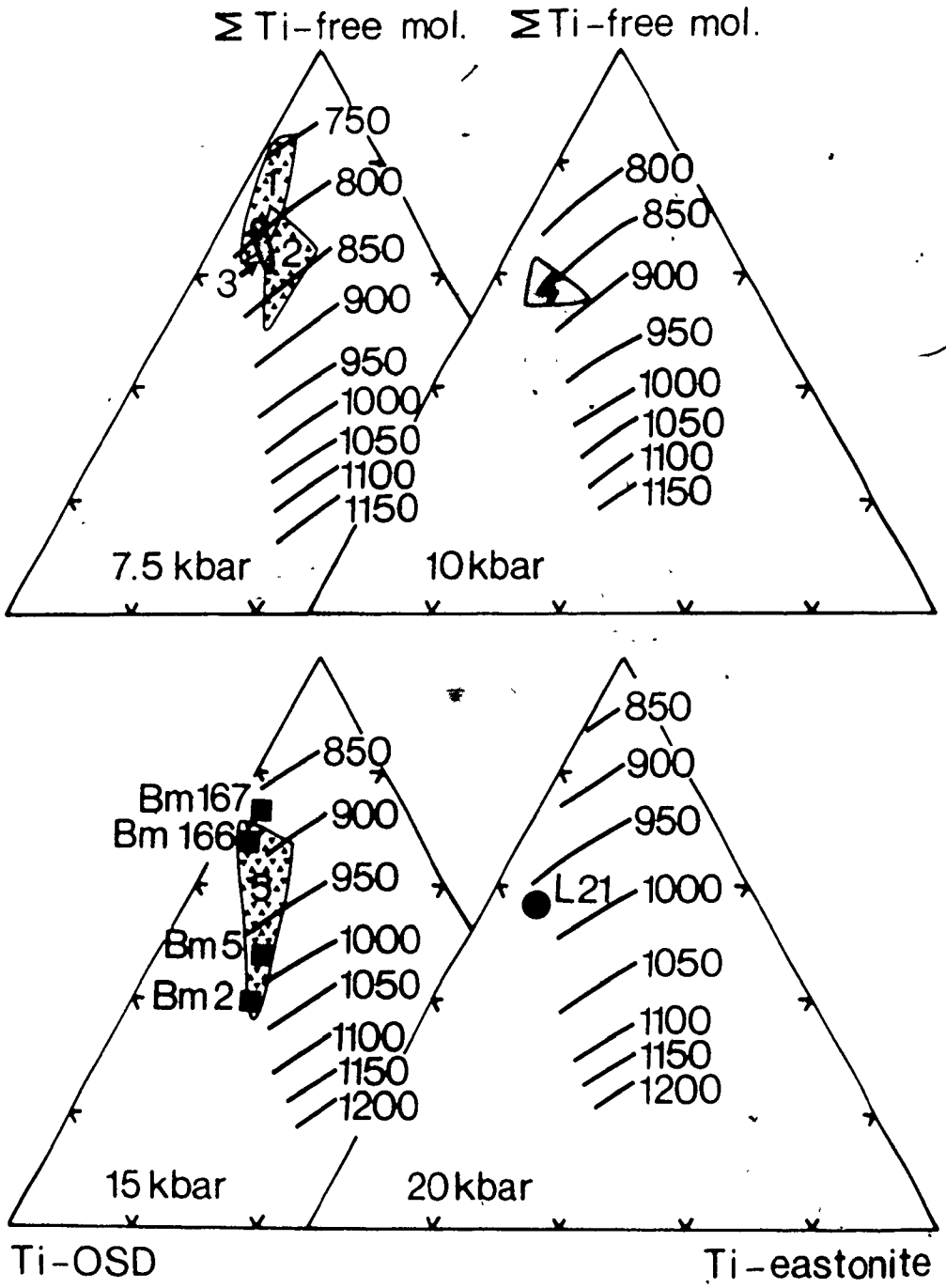
Σ Ti-free mol.
Σ Ti-free mol.
750
800
850
900
950
1000
1050
1100
1150
1
2
3
7.5 kbar
10 kbar
800
850
900
950
1000
1050
1100
1150
850
900
950
1000
1050
1100
1150
1200
Bm167
Bm 166
Bm 5
Bm 2
L21
15 kbar
20 kbar
Ti-OSD
Ti-eastonite

Figure 13b. Isobaric diagrams (25, 30, 35 and 45 kbar) contoured for temperature. Symbols as in Fig. 13a.

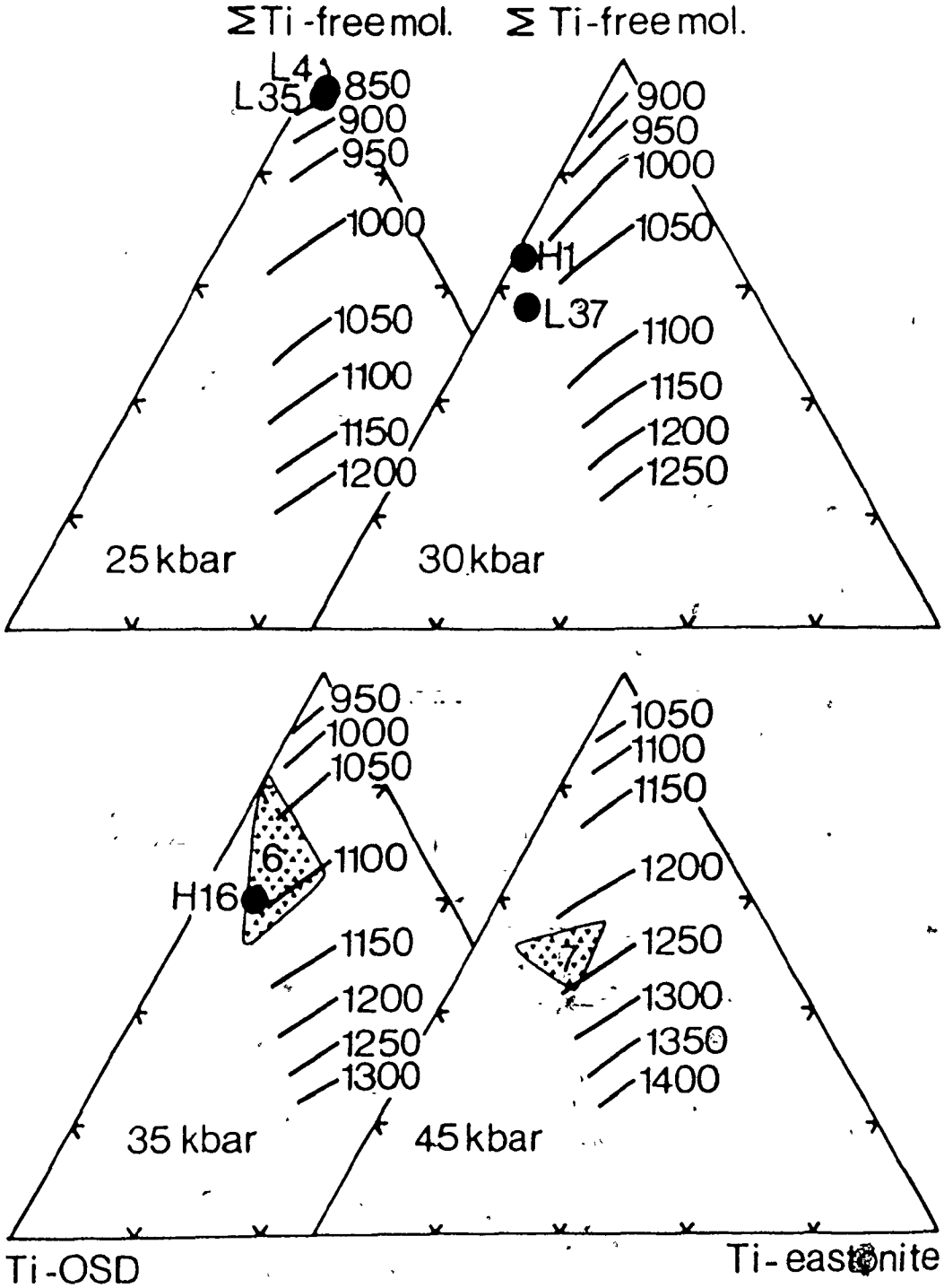
Σ Ti-free mol.
Σ Ti-free mol.
L4
L35
850
900
950
1000
1050
1100
1150
1200
H1
L37
900
950
1000
1050
1100
1150
1200
1250
25 kbar
30 kbar
950
1000
1050
1100
1150
1200
1250
1300
H16
6
35 kbar
1050
1100
1150
1200
1250
1300
1350
1400
7
45 kbar
Ti-OSD
Ti-eastonite

Figure 14a. Isothermal diagrams (750, 850, 900 and 950°C) contoured for pressure. Symbols as in Fig. 13a.

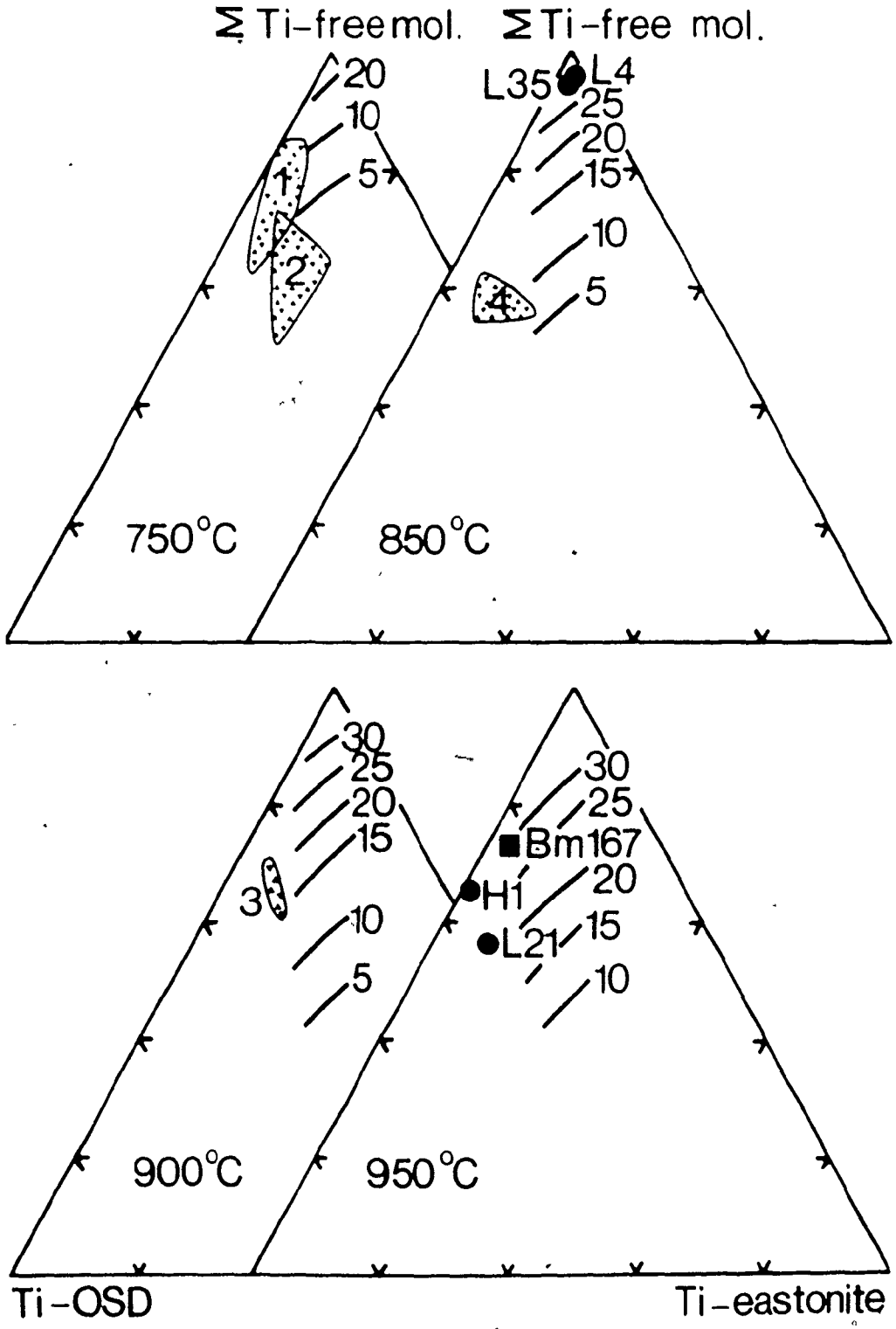
Σ Ti-free mol.
Σ Ti-free mol.
20
10
5
1
2
L35
L4
25
20
15
10
5
4
750°C
850°C
30
25
20
15
3
10
5
30
25
Bm167
H1
20
L21
15
10
900°C
950°C
Ti-OSD
Ti-eastonite

Figure 14b. Isothermal diagrams (1000, 1050 and 1100°C) contoured for pressure. Symbols as in Fig. 13a.

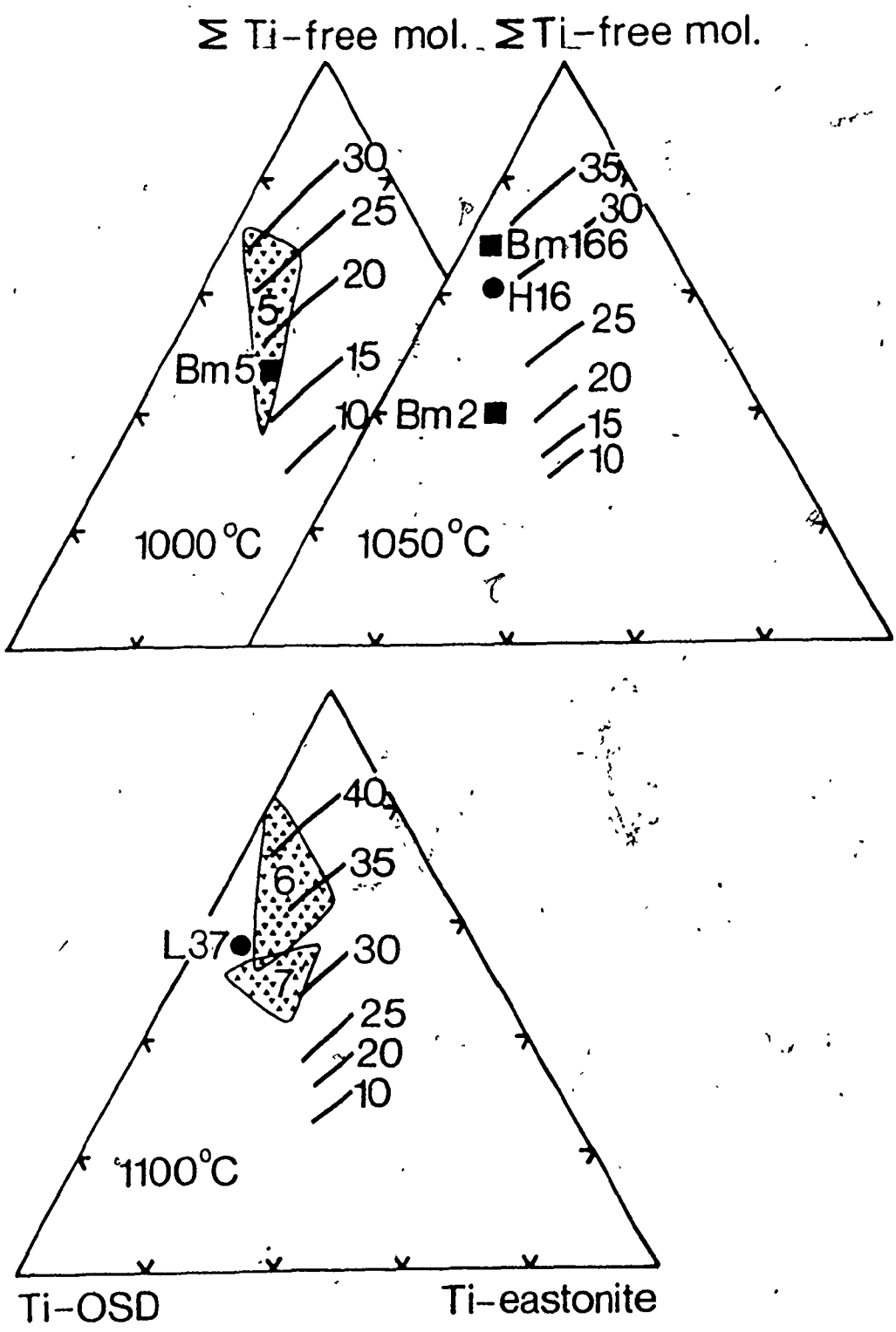
Σ Ti-free mol.
Σ Ti-free mol.
30
25
20
5
15
10
Bm5
1000 °C
35
30
Bm166
H16
25
20
15
10
Bm2
1050 °C
40
35
6
L37
30
7
25
20
10
1100°C
Ti-OSD
Ti-eastonite

were constructed. The contours are based on the single phase phlogopite compositions at the intersection of the TiO_2 solubility lines (Fig. 2) with the temperature and pressure of interest, and on the temperature-pressure coordinates of phlogopites coexisting with rutile.

Some extrapolations have been made to temperatures and pressures outside the range of the experiments (Fig. 13 and 14). This seems to be justified on the basis of the regularity in the variation of the TiO_2-content as a function of temperature and pressure within the investigated experimental range.

By plotting recalculated phlogopite compositions in Fig. 13 and 14, respectively, temperature and pressure determinations can be derived. To evaluate the accuracy of this phlogopite-geothermobarometer, the compositions of phlogopites from rocks with independent geothermometers and geobarometers were plotted in these diagrams, and the derived temperatures and pressures were compared to the independently determined T-p values (Tables 3, 4). Phlogopites which are suspected to have formed under conditions different from the temperatures and pressures based on the independent geothermometers and geobarometers were excluded from the evaluation.

Table 3a. Pressure and temperature determinations for phlogopites (Si+Al+Cr $\geq$ 8) in upper mantle xenoliths (the footnotes are in Table 3b).

Locality, Reference	Rock type, coexisting Ti-rich oxide (sample no.)	Ti-OSD (mol. %)	Ti-east (mol. %)	Mg/(Mg+Fe)	Independent p-T estimates[1] p (kbar)	T (°C)	Methods[3]	Phlogopite geothermobarometer[2] p (kbar)	T (°C)	Range
Premier Mine, S. Africa	Grt. lherzolite	41.9	7.0	0.91	46 ± 5	1100 ± 100	a,A	35	1200	29-35 kbar
Danchin (1979)		36.2	20.3	0.87				29	1260	1200-1260°C
		24.6	19.6	0.90				32	1225	
Navajo volc. field, USA	Grt. lherzolite, rutile	26.2	9.6	0.83	36 ± 4	1090 ± 140	b,B	37	1080	33-43 kbar
Ehrenberg (1982)		21.0	10.2	0.85				37.5	1070	1000-1120°C
		25.1	7.5	0.84				38	1065	
		18.3	17.4	0.82				34	1105	
		35.4	11.7	0.83				33	1120	
		30.4	8.1	0.90				37	1080	
		17.6	5.4	0.91				41	1040	
		18.4	0.1	0.92				43	1000	
		19.6	9.4	0.89				38	1065	
Hanaus/Lowrensia,	Grt. lherzolite (L37)	36.7	6.9	0.88	31.6	1105	c,B	36	1040	
Namibia, Mitchell (1984)	(L4)	1.2	3.1	0.94	26.5	855	c,B	30	840	
	(L21)	35.1	8.5	0.91	21.1	946	c,B	22	970	
	(L35)	2.5	2.8	0.93	26.8	841	c,B	29	840	
	(H1)	33.1	1.5	0.90	30.7	931	c,B	30	980	
	(H16)	31.0	8.7	0.89	35.2	1041	c,B	31	1080	
Victoria, Australia	Harzburgite (Bm2)	41.2	18.9	0.81	15	1035 ± 20	d,B,C,D	23	1010	
Griffin et al. (1984)	Lherzolite (Bm6)	35.5	17.1	0.81	14	1000 ± 20	d,B,C	18	980	
	Grt. pyroxenite (Bm166)	27.7	4.3	0.80	17 ± 3	1070 ± 130	c,e,f,B,C,E,F	34	890	
	Sp.-grt. pyrox (Bm167)	23.1	3.7	0.86	13.6	915 ± 115	c,e,f,B,C,E,F	30	870	
Victoria, Australia	Spinel lherzolite	27.4	1.4	0.91	14 ± 2	1000 ± 25	g,B	32	870	15-32 kbar
Nickel & Green (1984)		21.2	12.1	0.90				25	910	870-1030°C
		42.7	20.9	0.90				15	1080	

Table 3b. Pressure and temperature determinations for phlogopites (Si+Al+Cr $\geq$ 8) in lower crustal granulites.

Locality, Reference	Rock type, coexisting Ti-rich oxide	Ti-OSD (mol. %)	Ti-east (mol. %)	Mg/(Mg+Fe)	Independent p-T estimates[1] p (kbar)	T (°C)	Methods[3]	Phlogopite geothermobarometer[2] p (kbar)	T (°C)	Range
Enderby Land, Antarctica	Sapphirine bearing	25.4	5.3	0.96	7 ± 1	900 ± 30	h,B,C	21	780	14-21 kbar
Grew (1980)	granulite, rutile	27.5	11.3	0.96				14	830	780-830°C
Godthab, Greenland	Orthopyroxene gneiss,	11.6	3.0	0.77	7.5	750	i	11	750	4-12 kbar
Dymek (1983)	rutile and ilmenite	15.4	0.3	0.79				12	740	740-810°C
		19.3	5.2	0.83				7.5	775	
		21.1	7.8	0.74				6	790	
		21.5	8.2	0.82				5	795	
		22.0	8.2	0.76				5	795	
		25.9	7.6	0.75				4	805	
		31.3	6.2	0.73				4	810	
	Mafic, two-pyroxene	21.7	5.4	0.83	7.5	750	i	7	770	<3-7 kbar
	granulite, ilmenite	17.9	17.9	0.71				<3	850	770-870°C
		27.4	10.3	0.75				3	825	
		33.9	16.2	0.68				<3	870	
Pikwitonei, Canada	Sapphirine bearing	37.7	8.0	0.77	9 ± 1	830 ± 50	c,j,k,G	7	890	7-13 kbar
Arima & Barnett (1984)	granulite, rutile	27.7	16.9	0.78				11	850	800-890°C
		32.5	5.2	0.84				13	800	

Footnotes for Table 3a and 3b: 1. Where a range of determinations are indicated (±), the given value is the median value of the estimated range. 2. The temperatures are obtained from Fig. 13 using isobaric diagrams in accordance with the independent pressure estimates, and the pressures are obtained from Fig. 14 using isothermal diagrams corresponding to the independent temperature estimates. 3. Independent geobarometers and geothermometers: a: MacGregor (1974); b: Perkins & Newton (1980); c: Wood (1974); d: estimate based on the Victoria geotherm; e (and E): Herzberg (1978); f (and F): Ellis & Green (1979); g: Harley & Green (1982); h: Ghent (1976); i: see Dymek (1978); j: Newton & Haselton (1981); k: Newton & Perkins (1982); A: Davis & Boyd (1966); B: Wells (1977); C: Wood & Banno (1973); D: Lindsley & Dixon (1976); H: Anastasiou & Seifert (1972).

Table 4. The phlogopite geothermobarometer versus other independent temperature and pressure determinations. ΔT and Δp are deviations of the T and p values based on the individual phlogopite analyses from the median value of the independent determinations (see Table 3).

	No. of analyses	ΔT			Δp		
		<5%	5-20%	>20%	<5%	5-20%	>20%
Mantle xenoliths	25	16	9	0	5	11	9
Granulites	17	6	11	0	1	1	15
Total	42	22	20	0	6	12	24

5.2 Application of the phlogopite geothermobarometer to mantle xenoliths and lower crustal granulites

Fig. 13 and 14 and Tables 3 and 4 show that the determinations based on the phlogopite geothermobarometer are generally in good agreement with the independently estimated values for the mantle xenoliths (25 analyses) and granulites (17 analyses) used in the assessment.

5.2.1 Mantle xenoliths

The xenoliths equilibrated in the 30-45 kbar range show the same degree of agreement between the T-p values of the phlogopite geothermobarometer and the independent geothermometers and geobarometers as the xenoliths equilibrated in the 10-30 kbar range (Table 3). The temperature determinations from the phlogopite geothermobarometer show a remarkable agreement with the independent geothermometers. Although the pressure estimates do not show the same degree of coincidence, a majority of them deviate with less than 20% of the total pressure (Tables 3, 4).

5.2.2 Lower crustal granulites

The granulites cover the 5-10 kbar pressure range, just below the range of pressures used in the experimental study. As for the mantle xenoliths, the temperature determinations are in better agreement with the independently estimated values than the pressure determinations

(Table 4). The discrepancies between the values derived from the phlogopite geothermobarometer and the independent temperature and pressure determinations are somewhat larger for the granulites than for the mantle derived xenoliths.

5.3 Application of the phlogopite geothermobarometer to phlogopites crystallized in experiments on ultrapotassic rock compositions

The compositions of phlogopites crystallized from a melt in experiments on ultrapotassic rock compositions (Edgar et al., 1976, 1980; Barton & Hamilton, 1979; Arima & Edgar, 1983a, b) were plotted in triangular diagrams similar to Fig. 13 and 14 (not included in the thesis). The derived pressure and temperature estimates are given in Table 5. In spite of the tendencies to positive correlation between the TiO_2-contents of phlogopite and the temperature and negative correlation between the TiO_2-content of phlogopite and the pressure (Edgar et al., 1976; Arima & Edgar, 1981, 1983*b* and Table 5), the application of the experimentally developed phlogopite geothermobarometer results in temperatures and pressures that are consistently too low and too high, respectively. This relationship is in accordance with the lower TiO_2-contents in these supra-solidus phlogopites than in the subsolidus phlogopites from the present experimental study at the same pressure and temperature conditions.

Table 5. Pressure and temperature determinations for phlogopites crystallized during melting experiments with ultrapotassic rock compositions.

Rock type / Reference	Coexisting Ti-rich oxide	Ti-OSD	Ti-east	Ti-free mol.	East	Mg/(Mg+Fe)	wt. % H_2O added	Run conditions p (kbar)	Run conditions T (°C)	Phlogopite geothermobarometer[1] p (kbar)	Phlogopite geothermobarometer[1] T (°C)
Biotite mafurite		27.4	13.3	59.3	-	0.84	15	10	1050	28	870
Edgar et al. (1976)		14.6	12.2	73.2	0.4	0.90	10	10	1100	37	820
		14.4	12.2	73.4	0.8	0.90	15	10	1100	37	820
		32.8	9.7	57.5	5.7	0.89	5	10	1150	40	850
		14.5	7.8	77.7	5.0	0.90	15	20	1100	40	905
		21.4	3.0	75.6	6.7	0.90	15	20	1150	45	895
		27.6	6.4	66.0	6.7	0.90	5	20	1200	48	950
		27.3	12.1	60.6	12.3	0.91	5	20	1250	49	975
		10.4	6.9	82.8	14.8	0.83	40	30	1050	37	975
		16.7	1.5	81.8	11.8	0.86	15	30	1100	43	920
		14.9	5.3	79.7	6.8	0.89	15	30	1150	46	975
		13.3	0.4	86.3	12.2	0.92	15	30	1175	52	900
		13.4	0.5	86.1	11.8	0.92	15	30	1175	52	900
		27.3	14.8	57.8	0.6	0.82	5	30	1200	43	1070
		40.6	2.5	56.9	8.3	0.83	5	30	1250	54	1010
Madupite		33.4	3.4	63.2	-	0.91	-	20	1245	55	925
Barton & Hamilton (1979)											
Olivine ugandite		27.4	13.3	59.3	-	0.84	15	10	1050	28	870
Edgar et al. (1980)		15.2	4.8	80.1	14.5	0.86	25	20	1100	42	890
Katungite		19.0	8.0	73.0	-	0.88	15	12.5	1025	31	840
Arima & Edgar (1983a)		13.4	1.4	85.2	5.7	0.89	15	15	1050	40	825
		11.2	6.8	82.0	-	0.88	15	20	1050	36	890
		7.4	0.1	92.5	6.7	0.90	15	30	1125	49	850
		4.7	11.6	83.7	8.3	0.88	5	30	1200	50	1000
Wolgidite		51.8	6.2	42.0	-	0.98	13	10	950	22	870
Arima & Edgar (1983b)		58.9	2.9	38.0	-	0.95	13	15	1050	28	930
		45.1	0.7	45.1	-	0.92	13	20	1000	28	940
		33.6	2.2	64.1	-	0.95	13	20	1075	34	920
		29.4	1.5	69.1	-	0.93	13	22	1075	35	920

The temperatures are obtained from isobaric diagrams similar to Fig. 13, whereas the pressures are obtained from isothermal diagrams similar to Fig. 14.

CHAPTER 6

DISCUSSION

6.1 The effects of additional parameters on the solubility of Ti in phlogopite

The proposed geothermobarometer based on the solubility of Ti in phlogopite is derived from experiments with simplified synthetic starting materials. Although the starting compositions contain varying amounts of TiO_2, all of them (except those for the exploratory runs on the Ti-OSD and the Ti-eastonite molecules) have a Ti-OSD/Ti-eastonite ratio of unity (Fig. 1). In this section the influence of other parameters on the solubility of Ti in phlogopite is discussed. These parameters include variations in major element bulk composition, the presence or absence of separate coexisting Ti-rich oxides, the effects of additional elements (especially Fe) and the effects of variations in the oxygen fugacity of phlogopite crystallization.

6.1.1 Bulk composition

The experimental study shows that the TiO_2-content of phlogopite coexisting with rutile is not entirely determined by the pressure and temperature of equilibration, but is also influenced by the bulk composition of the system (Section 4.2; Fig. 7). Ti is predominantly incorporated by the Ti-OSD and the Ti-eastonite end members (Section 4.2 and 4.3), which have identical atomic proportions of K, Ti, H and O and relatively similar atomic proportions of Mg and Si. However, the Al/K ratios of the Ti-OSD and Ti-eastonite are 1 and 2, respectively. Thus the bulk Al_2O_3/K_2O, Al_2O_3/TiO_2, Al_2O_3/MgO, Al_2O_3/SiO_2 and Al_2O_3/H_2O ratios of the system will control the relative proportions of these two molecules. At a given temperature and pressure a high activity of Al_2O_3 will favour a high proportion of the Ti-eastonite molecule relative to the Ti-OSD molecule in the phlogopite.

As shown by the experiments the relative abundance, and thus the relative stability, of the Ti-eastonite end member in phlogopite is lower than that of the Ti-OSD end member (Fig. 7). An increase in the proportion of Al in the bulk system will therefore lead to a decrease of the solubility of Ti in phlogopite. The exploratory experiments performed with the Ti-OSD and the Ti-eastonite molecules as starting materials confirm this tendency (Table 2, Fig. 7).

In rocks without Al-rich minerals, such as spinel and garnet, the amount of Al available to phlogopite formation will be roughly proportional to the total Al-content of the rock. However, when such Al-rich phases are present the available Al for phlogopite formation will be buffered by these minerals (Arai 1984).

6.1.2 Bulk TiO_2-content and the presence of Ti-rich oxides

The presence of Ti-rich oxide minerals, such as rutile and ilmenite, in a given mineral assemblage indicates that the bulk system contains more TiO_2 than the amount which can be accommodated in the silicate minerals, as well as in magnetite and spinel.[1] The experimentally developed phlogopite geothermobarometer is based on phlogopites co-existing with rutile, whereas only 5 of the 17 mantle xenoliths and granulites used in the assessment of the geothermobarometer (Table 3) contain a separate Ti-rich oxide (rutile or ilmenite).

However, the absence of Ti-rich oxides in many of the samples does not appear to result in any increased deviation of the temperature and pressure determinations of the phlogopite geothermobarometer from the determinations based on independent geothermometers and geobarometers. The reason for this may be that even the phlogopites with-

[1] The mineral assemblage is saturated with respect to TiO_2 according to the terminology used by Guidotti (1984) and Ghent & Stout (1984).

out observed coexisting Ti-rich oxides are close to saturation with respect to TiO_2.

6.1.3 Ferrous iron

The only octahedral divalent cation in the phlogopites of the simplified synthetic system is Mg^{2+}. Other divalent cations, in particular Fe^{2+}, are expected to exert additional control on the solubility of Ti in phlogopite. The substitution of Fe^{2+} (octahedral ionic radius of 0.78A; Shannon, 1975) for Mg^{2+} (radius of 0.72A) will increase the size of the octahedral layer, and thus reduce the misfit between the octahedral and tetrahedral layers (Bailey, 1984). The reduction of the crystallographical misfit by the incorporation of Fe^{2+} will make the phlogopite structure susceptible to larger proportions of the Ti-OSD and the Ti-eastonite end members (section 4.4), and explains the positive correlation between the Fe/Fe+Mg ratio of phlogopite and the solubility of Ti in the mineral (Guidotti et al., 1977; Ghent & Stout, 1984).

Increasing TiO_2-contents as a function of increasing Fe/(Mg+Fe) ratios of phlogopites have been observed both in high-grade metamorphic rocks (Guidotti et al., 1977; Dymek, 1983) and in mantle xenoliths, kimberlites and ultrapotassic rocks (Dawson & Smith, 1975; Smith et al., 1978; Delaney et al., 1980; Van Kooten, 1980; Mitchell, 1981; Bachinski & Simpson, 1984). The phlogopites used for the

assessment of the experimentally developed geothermobarometer have Mg/(Mg+Fe) ratios ranging from 0.68 to 0.96 (Table 3). The variation of the ratios within this range does not seem to affect the accuracy of the phlogopite geothermobarometer significantly. However, a tendency to positive correlation between the Mg/(Mg+Fe) ratio and the pressure and negative correlation between Mg/(Mg+Fe) and the temperature can be observed for the analyses of the phlogopites from the West Greenland granulites (Table 3).

6.1.4 Oxygen fugacity - ferric iron

Variations in oxygen fugacity may result in changes in the oxidation states of some of the elements present in phlogopite. As pointed out in section 1.3, Ti is most likely quadrivalent (in mica as well as other minerals) under all conditions relevant to the lower crust and upper mantle, whereas Fe may be both divalent and trivalent. An Fe-free system was chosen for the present experimental study, partly to avoid the uncertainties related to different oxidation states of Fe.

Arima & Edgar (1981) pointed out that the phlogopites crystallized under high oxygen fugacity (HM buffer) during melting experiments on a biotite mafurite composition (Ryabchikov & Green, 1978) have higher Ti-contents than those formed from the same rock composition under lower oxygen fugacity (NNO buffer, Edgar et al., 1976). These

results indicate that the oxygen fugacity may be one of the important factors influencing the solubility of Ti in phlogopite.

As shown in section 4.3 (Fig. 8b) Ti is incorporated into phlogopite in the form of the Ti-OSD and the Ti-eastonite end members even in the phlogopites with a tetrahedral site deficiency (Si+Al+Cr < 8). Since Ti does not seem to occupy the tetrahedral site in these phlogopites, the assumption that ferric iron fills up the vacant tetrahedral sites appears to be justified. This implies that ferric iron is present at least in sufficient amounts to fill the tetrahedral sites, and that a correspondingly high oxygen fugacity prevailed during the equilibration of these phlogopites.

6.2 Geothermometry versus geobarometry

The slope of the most accurately constrained TiO_2 solubility line (composition B) is about 0.13 kbar/°C (Fig. 2). The slopes of the solubility lines for the other three compositions appear to vary between 0.10 kbar/°C and 0.14 kbar/°C. Most of the lower crustal and upper mantle mineral transformations have also positive pressure-temperature slopes (e.g. overviews by Griffin and Heier, 1973; Carswell, 1980; and Bohlen et al., 1984). However, the experimentally determined slopes of the solubility lines for TiO_2 in phlogopite are considerably steeper than

the slopes of these mineral transformations.

Most of the pressure-temperature slopes of the subsolidus intermineral partitioning coefficients commonly used as geothermometers and geobarometers are also positive (e.g. MacGregor, 1974; Råheim and Green, 1974; Mori and Green, 1978; Adams and Bishop, 1982; Harley and Green, 1982; Johnson et al., 1983; Harley, 1984). Typically, the slopes of the geothermometers and geobarometers ranges from 0.10 to 0.20 kbar/°C and from 0.03 to 0.07 kbar/°C, respectively. A slope of 0.10-0.14 kbar/°C for the solubility of TiO_2 in phlogopite therefore indicates greater geothermometric than geobarometric potentials.

6.3 Comparison between the phlogopite geothermobarometer and other geothermometers and geobarometers

The independent temperature and pressure determinations used in the assessment of the phlogopite geothermobarometer were derived from a variety of geothermometers and geobarometers. Most of the independent temperature determinations are based on different formulations of the diopside-enstatite solvus geothermometer (Davis & Boyd, 1966; Ross et al., 1973; Wells, 1977; Lindsley & Dixon, 1976; Mori, 1978), whereas most of the pressure determinations are based on the solubility of Al_2O_3 in orthopyroxene (Anastasiou & Seifert, 1972; MacGregor, 1974; Wood, 1974;

2 OF / DE 2

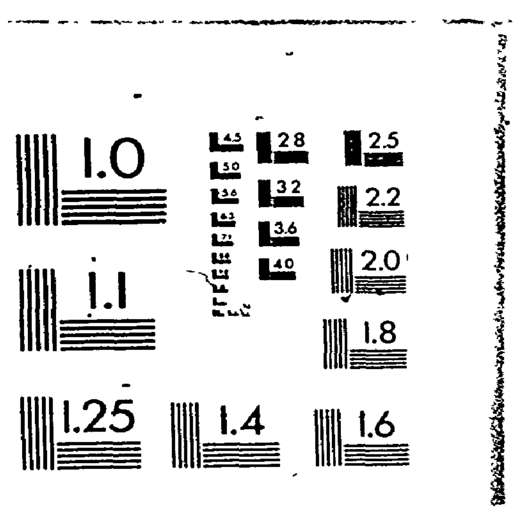

Arima, 1978; Danckwerth & Newton, 1978; Perkins & Newton, 1980; Harley & Green, 1982). It is beyond the scope of this study to assess the quality of these various formulations. However, most of the new contributions to a geothermometer or geobarometer represent an improvement in the form of more accurate consideration of the effects of additional parameters, e.g. minor elements.

The phlogopite geothermobarometer shows especially good agreement with the Wells (1977) pyroxene solvus geothermometer and the Wood (1974) geobarometer for the Namibian mantle xenoliths (Mitchell, 1984; Table 3). Good agreement is also found for the Navajo Volcanic Field mantle xenoliths for which independent temperatures and pressures were derived from the Wells (1977) and Mori (1978) geothermometer and the Perkins & Newton (1980) geobarometer (Ehrenberg, 1982). Larger discrepancies are encountered for the Premier Mine kimberlite mantle xenoliths for which the temperatures and pressures were independently determined by the Davis & Boyd (1966) geothermometer and the MacGregor (1974) geobarometer (Danchin, 1979). The David & Boyd (1966) and MacGregor (1974) formulations have been revised (e.g. Wells, 1977 and Wood, 1974), and it is likely that part of the discrepancies can be ascribed to the inadequacies of the original geothermometers and geobarometers.

The application of various geothermometers and geo-

barometers to suites of lower crustal or upper mantle rocks often results in a range of temperatures and pressures (e.g. Ehrenberg, 1982). In such cases the phlogopite geothermobarometer may help to restrict the probable temperature and pressure ranges (e.g. Navajo Volcanic Field, Table 3).

6.4 Suprasolidus crystallization of phlogopite

The application of the phlogopite geothermobarometer to the phlogopites crystallized during the melting experiments on ultrapotassic rock compositions systematically gives lower temperatures and higher pressures than the experimental temperatures and pressures (Table 5). These discrepancies, which are a consequence of low Ti-contents in the suprasolidus phlogopites, can probably be ascribed to differences between the crystal-melt partitioning of Ti in the melting experiments and the intermineral subsolidus partitioning of Ti in the present experimental study.

The suprasolidus runs on composition A in the present study indicate phlogopite-melt partitioning ratios of Ti of less than unity (phlogopite and glass analyses in Table 2). In these suprasolidus experiments the Ti-content of phlogopite appears to decrease with increasing temperature (Fig. 2). The low phlogopite-melt partitioning ratios of Ti in the suprasolidus runs are in accordance with the systematic deviations of the T-p values derived from the

subsolidus phlogopite geothermobarometer and the temperatures and pressures of the melting experiments. The locations and the directions of the phase boundaries and the solidi lines in Fig. 3 also suggest that the subsolidus phlogopite geothermobarometer can not be extrapolated to suprasolidus conditions.

In volcanic and subvolcanic rocks, the phlogopite phenocrysts are commonly higher in Ti than the whole rocks (Carmichael, 1967; Ellis, 1976; Brooks et al., 1978; Duda & Schminke, 1978; Edgar, 1979; Sheraton & Cundari, 1980; Van Kooten, 1980; Baldridge et al., 1981; Melver, 1981; Hall, 1982; Clarke et al., 1983; Edgar & Arima, 1983; Scott Smith & Skinner, 1984; Irving & Frey, 1984) in spite of the observed phlogopite-melt partitioning ratios of less than unity. This may largely be a result of early crystallization of Ti-poor phases and/or near solidus or subsolidus reequilibration of the phlogopite phenocrysts.

6.5 Petrological implications

6.5.1 Phlogopite versus chain silicates as reservoirs for TiO_2 in the mantle and the lower crust

Phlogopite and amphibole are the two major hydrous minerals in the upper mantle and the lower continental crust. Along with clinopyroxene these minerals are also major silicate reservoirs for TiO_2. Both H_2O and TiO_2 are important components of mantle xenoliths enriched in large

ion lithophile elements by metasomatism or melt infiltration (Bailey, 1982).

In lower crustal and upper mantle rocks the Ti-content is generally considerably higher in phlogopite than in the coexisting amphiboles and pyroxenes (Dawson & Smith, 1975; Wilkinson, 1975; Ellis, 1976; Clifford et al., 1981; Jones et al., 1982; Griffin et al., 1984; Nickel & Green, 1984). This may be explained by the different modes of incorporation of Ti in these minerals. In phlogopite, Ti is predominantly incorporated by the Ti-OSD molecule, and partly by the Ti-eastonite molecule (Chapter 4). However, the chain silicate structures do not allow as large octahedral site vacancies as the trioctahedral mica structure (Deer et al., 1978). In amphiboles and pyroxenes, Ti is mainly incorporated by the Ti-tschermak substitution; $Mg_2Si = Ti_2Al$ (Deer et al., 1978; Oba et al., 1984; Otten, 1984).

Ti-rich pyroxenes and amphiboles with high Al/Si ratios and high Al^{IV}/Al^{VI} ratios are common in igneous rocks of low pressure origin, but they generally break down at higher pressure to form Ti-poor pyroxenes and amphiboles coexisting with a Ti-rich oxide, commonly rutile (Griffin & Heier, 1973; Dawson & Smith, 1982; Oba et al., 1984).

The limited stability at high pressure of the Ti-rich pyroxenes and amphiboles with high proportions of the Ti-tschermaks and the Ti-tschermakite molecules is consistent with the low proportions of the Ti-eastonite molecule in

the high pressure phlogopites (Chapter 4).

6.5.2 Availability of Ti - mantle enrichment

Carswell (1975) and Delaney et al. (1980) divided phlogopites from mantle xenoliths into primary textured and secondary textured types. The primary textured phlogopites generally contain less than 0.5 wt. % TiO_2 and do not coexist with Ti-rich oxides, whereas the secondary textured phlogopites have higher TiO_2-contents and often coexist with Ti-rich oxides.

The present experimental study and the studies of Forbes & Flower (1974), Danchin (1979) and Ehrenberg (1982) have shown that phlogopites equilibrated at pressures of even 30 kbar or more often contain at least 2-4 wt. % TiO_2. The primary textured phlogopites of Carswell (1975) and Delaney et al. (1980), containing less than 0.5 wt. % TiO_2, have therefore most likely equilibrated in an environment with limited supply of TiO_2. If the primary textured phlogopites represent the common type of phlogopite in primordial or in depleted regions of the upper mantle, a Ti-enrichment process (metasomatism or melt infiltration) may be required to produce the Ti-rich secondary phlogopites.

Since secondary phlogopite is one of the most important minerals in enriched mantle regions (Bailey, 1982; Harte, 1983), this geothermobarometer may contribute

to a better understanding of the physical conditions and depths of mantle metasomatism and melt infiltration processes.

CHAPTER 7

CONCLUSIONS

The main conclusions of the study are:

1. The solubility of Ti in phlogopite increases systematically with increasing temperature and decreases systematically with increasing pressure in the investigated range from 10 to 30 kbar and from 825°C to 1300°C.
2. For a given starting composition the low-Ti phlogopites coexisting with rutile have lower proportions of the Ti-eastonite end member molecule and higher proportions of the eastonite molecule than the high-Ti single phase phlogopites. The variations in the proportions of the phlogopite and the Ti-OSD end members with variations in temperature and pressure are minor.
3. Phlogopites in mantle xenoliths, mantle derived volcanic rocks and lower crustal granulites have

similar relative proportions of the end member molecules phlogopite, eastonite, Ti-OSD and Ti-eastonite as the experimentally produced phlogopites of synthetic composition. In phlogopites with Si+Al+Cr < 8 the tetrahedral sites appear to be occupied by Fe^{3+} rather than by Ti.

4. The phlogopite geothermobarometer developed on the basis of the experimental results gives T-p values in good agreement with independent T-p determinations from mantle xenoliths and lower crustal granulites. The accuracy of the temperature estimates is better than the accuracy of the pressure determinations. Further refinements of the phlogopite geothermobarometer, including evaluations of the effects of Fe and possibly other minor elements such as Na, Ba and Cr, may provide a powerful tool for the determinations of the temperature and pressure conditions of phlogopite formation in the upper mantle and the lower crust.

5. The proposed geothermobarometer is based on a subsolidus experimental investigation, and can not be extrapolated to suprasolidus conditions.

6. Phlogopites with high proportions of the Ti-OSD molecule are stable in the lower crust and upper mantle, representing a major potential reservoir for Ti. Amphiboles and pyroxenes can normally not

accommodate as large amounts of Ti under high pressure conditions due to the limited possibilities of octahedral site deficiency in the chain structures.

APPENDIX 1

PREPARATION OF STARTING MATERIALS

Oxide and carbonate components

SiO_2: High-purity quartz provided by the Geophysical Laboratory, Carnegie Institution, Washington, D.C. Prepared by crushing to about 60 mesh in a steel mortar, removal of steel fragments by a strong magnet and by hand-picking, treatment with hot dilute H_2SO_4 and hot concentrated HCl solutions, washing with distilled water, grinding for ca. 1 hr in acetone, and roasting for ca. 2 hrs at 1500°C, to remove any fluid inclusions and convert it to cristobalite.

Al_2O_3: Fisher laboratory grade Al_2O_3
Prepared by roasting at 1400°C for 2 hrs

TiO_2: Fisher laboratory grade TiO_2

MgO: Fisher laboratory grade MgO

K_2CO_3: Fisher laboratory grade K_2CO_3

All the components were kept at 110°C for about 12 hrs before they were cooled in a desiccator and weighed to form the stoichiometric phlogopite compositions.

Preparation of the starting compositions

A total of 5-10 g of the oxides was prepared for each of the stoichiometric phlogopite compositions (Table 1). The oxide mixtures were ground in acetone in an agate mortar for about 30 minutes to ensure homogeneity and uniform grain size. After complete evaporation of the acetone, the material was transferred to a Pt-crucible and kept at 950°C for 30 minutes to convert K_2CO_3 to K_2O. No carbonate was detected by examination by HCl-solution and X-ray diffractometry after this initial heating.

Another grinding (30 min) in an agate mortar was followed by sintering of the material at 1050°C for 20 minutes and a final disaggregation and homogenization by light, manual crushing and grinding. The starting material was then dried at 110-120°C for about 12 hrs and cooled in a desiccator prior to filling of the sample capsules.

APPENDIX 2

PREPARATION OF SAMPLE CAPSULES

Sample capsules of $Ag_{50}Pd_{50}$ alloy and Pt metal were used in this study (Pt above 1225°C). After crimping, welding and annealing one of the ends of the ca. 7 mm long, 1 mm wide tubing, about 0.27 mg of distilled and deionized water was added with a microsyringe. The exact amount of water was estimated by weighing the capsule before and after the addition of water. The ideal amount of material in each sample capsule is 5 to 7 mg corresponding to 0.22 to 0.31 mg H_2O to form a stoichiometric phlogopite composition. If the weight of H_2O was outside the range of 0.24 to 0.30 mg, the capsule was heated to evaporate the water, and a new loading was performed.

The correct amount of anhydrous powder was then loaded into the capsule to form a stoichiometric phlogopite composition (95.7 wt. % anhydrous material). After cleaning the upper, inside wall of the capsule, the upper end was crimped and welded. Weighing was performed prior to and after the welding to ensure that no loss of water or material occurred during the welding operation. The capsule was then kept at a temperature of 110 to 120°C for

ca. 30 minutes, and reweighed to make sure that it was properly sealed. If no weight loss was detected the capsule was squeezed in a steel cylinder to the proper form for the high pressure cell assembly, held at 110 to 120°C for at least 10 hrs and reweighed prior to the experimental run.

The uncertainty of the weighing operation is estimated to be ± 0.02 to ± 0.03 mg from repeated weighing of the same sample. Due to the large ratio of anhydrous material to water, this uncertainty will mostly affect the water content. The table below shows the relations between the mass of water and the percentage of water for a given mass (6.00 mg) of anhydrous material.

Mass of H_2O [mg]	wt. % H_2O for 6.00 mg of anhydrous material
0.24	3.85
0.25	4.00
0.26	4.15
0.27	4.31
0.28	4.46
0.29	4.61
0.30	4.76

This table indicates that within the range from 0.24 mg to 0.30 mg water the weight percentage of water changes by 0.15% for each mass increment of 0.01 mg water mixed with a fixed mass of 6.00 mg anhydrous material. A weighing uncertainty of ± 0.02 to 0.03 mg will therefore result in an uncertainty of about 4.3 ± 0.4 wt. % H_2O.

APPENDIX 3

ANALYTICAL PROCEDURE

The phlogopite compositions were determined by electron microprobe on carbon coated polished sections where the disaggregated run products were embedded in epoxy. A Materials Analysis Company model 400 electron microprobe with three spectrometers and KRISEL automation was used. Due to the small grain size of the run products, the electron beam had to be highly focussed. However, the operating conditions were chosen to minimize volatilization of potassium as well as electron beam damage of the sometimes very thin surface edges of the phlogopite plates. At the same time the exitation voltage, sample current and counting time were maintained at a level sufficient to give acceptable counting statistics. An exitation voltage of 15 kV was used throughout, combined with a sample current of either 0.250 μA, 0.200 μA or 0.150 μA, and counting times of 30 s, 20 s or 10 s for each of the elements (1. step of peak seek and counting: K and Mg; 2. step: Al and Ti; and 3. step: Si). Continuous monitoring of the sample current on carbon eliminated corrections for drift. The raw data were subjected to background correction and corrections for mass absorption, fluorescence and atomic number effects by

the procedure (Magic IV) of Colby (1971). The standards used were in most cases an olivine (Fo_{91}) for Mg, a plagioclase (An_{90}) for Al, an orthopyroxene (En_{45}) for Si, an orthoclase for K and a kaersutitic amphibole (5.65 wt. % TiO_2) for Ti. The accuracy and precision were tested by analyzing some of the mineral standards, single phase phlogopite run products of known composition, as well as by repeated analyses of phlogopites from various run products (see Section 2.4).

APPENDIX 4

CALCULATION OF STRUCTURAL FORMULAE AND END MEMBER MOLECULES

Structural formulae

The cation proportions for the structural formulae are based on 22 oxygen atoms. Almost all of the phlogopites from the present experimental study and most of the phlogopites of natural composition have (Si+Al) $\geq$ 8. For those phlogopites with (Si+Al) < 8 a problem arises with respect to the assignment of additional cations to the tetrahedral site. In the very few (3) experimentally produced synthetic phlogopites with minor tetrahedral site deficiencies, Ti was assigned to fill this site (Table 2).

Cr was assigned to the tetrahedral site as the first element after Si and Al in the natural phlogopites with (Si+Al) < 8. This decision was made on the basis of its ionic size and crystal chemical properties (Shannon, 1976; Matzat & Shiraki, 1978). The controversy of whether Fe^{3+} or Ti^{4+} is present in the tetrahedral sites in the phlogopites with Si+Al+Cr < 8 was reviewed in Section 1.3. In order to realize the consequences of the choice of tetrahedral cations on the end member molecules, the structural formulae for the phlogopites with (Si+Al+Cr) < 8 were initially calculated by the following different

methods:

1. Ti was assigned to the tetrahedral site in preference to Fe. All of the Fe was assumed to be ferrous.
2. Fe was assigned to the tetrahedral site in preference to Ti. The tetrahedral Fe was assumed to be ferric, whereas the rest of the Fe was assumed to be ferrous.

Since the selected phlogopite analyses compiled from the literature were obtained by electron microprobe, only the total iron contents are known.

End member molecules

The purpose of the calculation of the end member molecules is to separate the Ti-free components of the phlogopite solid solutions from the Ti-OSD and the Ti-eastonite molecules. In the simplified synthetic phlogopites the Ti-free end members only include the phlogopite and the eastonite molecules, whereas natural phlogopites also contain Ti-free end members where Na, Ba, Ca, Fe, Mn, Ni and Cr are present.

The calculation of the end member molecules, performed by computer programs written in BASIC, was based on the structural formulae, and charge balance and stoichiometry were maintained during the calculation. Cations with identical charge and coordination number in the mica crystal structure were grouped together and summed in the following way (Bailey, 1984):

Interlayer cations: $X^{+} = K+Na$
$X^{2+} = Ba+Ca$

Octahedral cations: $Y^{2+} = Mg+Fe^{2+}+Mn+Ni$
$Y^{3+} = Al^{VI}+Cr^{VI}$
$Y^{4+} = Ti$
(Phlogopites with Si+Al+Cr<8: $Y^{4+} = Ti+Ti^{IV}$ if some of the Ti has been assigned to the tetrahedral sites)

Tetrahedral cations: $Z^{3+} = Al^{IV}+Cr^{IV}$
$Z^{4+} = Si$
(Phlogopites with Si+Al+Cr<8: $Z^{3+} = Al+Cr^{IV}+(Fe^{3+})^{IV}$ or $Z^{4+} = Si+Ti^{IV}$)

The first part of calculation of the end member molecules was performed separately for the phlogopites with Si+Al+Cr≥8 and for those with Si+Al+Cr<8. An example of the calculation procedure is given in Table A4.

A. Phlogopites with Si+Al+Cr ≥ 8

Step 1: Octahedral Al and Cr were combined with K, Mg and tetrahedral Cr, Al and Si to form the eastonite molecule:
$K_2[Mg_5(Al^{VI}Cr^{VI})][Si_5(Cr,Al)_3]O_{20}(OH)_4$

Step 2: Ba and Ca were combined with K, Mg, Al and Si to form the Ba-Ca-molecule: $(Ba,Ca)_2Mg_6Si_4Al_4O_{20}(OH)_4$ (Wendlandt, 1977; Gaspar & Wyllie, 1982; section 1.3)

B1. Phlogopites with Si+Al+Cr<8, structural formula with tetrahedral Ti

Step 1: Tetrahedral Ti was combined with K, Mg and Al to form the Ti^{IV}-molecule: $K_2Mg_6(Ti_6Al_2)O_{20}(OH)_4$

Step 2: as above (Ba-Ca-molecule)

B2. Phlogopites with Si+Al+Cr<8, structural formula with tetrahedral Fe^{3+}

Step 1: as step 2 above (Ba-Ca-molecule)

The remaining part of the calculation of end member molecules is common to all of the three categories (A, B1, B2). Both the Ti-OSD and the phlogopite-annite components have Al/Si ratios of 1/3, whereas the Ti-eastonite molecule has a Al/Si ratio of 1. The relations between the amount of Al and Si in the remaining end member molecules can be expressed in the following equations, where N^j_i is the amount of element i in component j:

$$N^{Ti\text{-east}}_{Si} = N^{Ti\text{-east}}_{Al},\quad N^{Ti\text{-OSD}}_{Si} = 3N^{Ti\text{-OSD}}_{Al},$$

$$N^{phl\text{-annite}}_{Si} = 3N^{phl\text{-annite}}_{Al} \qquad (1)$$

$$\Sigma N_{Si} = N^{Ti\text{-east}}_{Si} + N^{Ti\text{-OSD}}_{Si} + N^{phl\text{-annite}}_{Si} \qquad (2)$$

$$\Sigma N_{Al} = N^{Ti\text{-east}}_{Al} + N^{Ti\text{-OSD}}_{Al} + N^{phl\text{-annite}}_{Al} \qquad (3a)$$

$$N^{Ti\text{-OSD}}_{Al} + N^{phl\text{-annite}}_{Al} = \Sigma N_{Al} - N^{Ti\text{-east}}_{Al} \qquad (3b)$$

Combining equations 1 and 2 gives:

$$\Sigma N_{Si} = N^{Ti\text{-east}}_{Al} + 3(N^{Ti\text{-OSD}}_{Al} + N^{phl\text{-annite}}_{Al})$$

$$\Sigma Ni_{Si} = N^{Ti\text{-east}}_{Al} + 3(\Sigma N_{Al} - N^{Ti\text{-east}}_{Al})$$

$$N^{Ti\text{-east}}_{Al} = 1/2(3\Sigma N_{Al} - \Sigma N_{Si}) \qquad (4)$$

The Ti-eastonite molecule ($K_2Mg_5TiSi_4Al_4O_{20}(OH)_4$) was formed from the amount of Al derived from equation 4 along with the required K, Mg, Ti and Si. This adjusts the Al/Si ratio for the remaining molecules to 1/3.

The remaining Ti was then assigned to the Ti-OSD molecule ($K_2Mg_4TiSi_6Al_2O_{20}(OH)_4$). For some few analyses with very high TiO_2-contents (ca. 10 wt. %) and consequently high proportions of the Ti-eastonite and the Ti-OSD molecules (e.g. Mitchell 1981, Fig. 11b), some additional X^+ and Y^{2+} ions other than K and Mg was required to form the Ti-OSD molecule.

The remaining elements were assigned to a phlogopite-annite component ($X^+Y^{2+}(Si_6Al_2)O_{20}(OH)_4$) based on the intermediate value of the remaining X^+, $Y^{2+}/3$ and Al = Si/3 (Al = Si/3 is normally intermediate, whereas X^+ is mostly the smallest and $Y^{3+}/3$ is mostly the largest value). The residuals (the sum of the absolute values of the residuals) after the formation of the phlogopite-annite component (mostly positive residuals for Y^{2+} and negative residuals for X^+) are generally less than 2% of the total amount of cations.

In addition to the sequence of end members reviewed above, the annite molecules $K_2Fe^{2+}Si_6Al_2O_{20}(OH)_4$ and $K_2(Fe^{2+},Mn,Ni)_6Si_6Al_2O_{20}(OH)_4$ were independently determined from the amount of Fe^{2+} and $Fe^{2+}+Mn+Ni$, respectively. The molar proportions of these molecules are 25-30% in the most Fe-rich phlogopites.

When these calculation procedures are followed, the calculated value of the Ti-eastonite molecule generally becomes negative (i.e. $(3x\ N_{Al} - N_{Si}) < 0$) for the phlogopites in category B1. On the basis of this relationship combined with the main objective of studying the octahedral substitution of Ti in phlogopite, the structural

formulae and end member molecules based on the assignment of Fe^{3+} rather than Ti to the tetrahedral sites were chosen for further consideration in Chapter 4. As shown in section 4.3 the assumption that Ti is confined to the octahedral sites even in phlogopites with Si+Al+Cr<8, is supported by the mineral chemistry of these phlogopites (Fig. 8b).

Table A4. Example of calculation of end member molecules for phlogopite analysis F077, Ehrenberg (1982), Table 8.

	Structural formula	Molecule 1 Eastonite	Molecule 2 Ca-Ba-mol	Remaining cations	Molecule 3 Ti-east	Molecule 4 Ti-OSD	Remaining cations	Molecule 5 Phl.-Ann.	Final residuals
Si	5.749	0.410	0.016	5.323	0.322	1.824	3.177	3.177	
Al	2.251	0.246	0.016	1.982	0.322	0.608	1.059	1.059	
Al	0.021	0.021							
Cr	0.061	0.061							
Ti	0.385			0.385	0.081	0.304			
Mg	4.750	0.410	0.024	4.316	0.403	1.216	2.697	2.265	+0.041
Fe	0.520			0.520			0.520	0.520	
Mn	0.001			0.001			0.001	0.001	
Ca	0.008		0.008						
Na	0.055			0.055			0.055	0.055	
K	1.851	0.164		1.687	0.161	0.608	0.918	1.004	-0.086
Sum tetr. cations	8.000	0.656	0.032		0.644	2.432		4.236	
Mol %	100.00	8.20	0.40		8.05	30.40		52.95	

The molecular proportions (mol %) of the end member molecules are based on the sum of the tetrahedral cations for each molecule.

APPENDIX 5

DATA SOURCES FOR PHLOGOPITE ANALYSES

The complete references are given in the list of references.

Mantle xenoliths: Aoki, 1975; Boettcher & O'Neil, 1980; Danchin, 1979; Dawson & Smith, 1973, 1975, 1977; Dawson et al., 1970; Delaney et al., 1980; Ehrenberg, 1979, 1982; Emeleus & Andrews, 1975; Exley et al., 1982; Farmer & Boettcher, 1981; Griffin et al., 1984; Harte & Gurney, 1975; Jones et al., 1982; Kay et al., 1983; Leavy, 1979; McIver, 1981; Mitchell, 1984; Nickel & Green, 1984; Prinz et al., 1975; Rimsaite, 1971.

Megacrysts and cumulate inclusions in kimberlites and alkaline volcanics: Aoki, 1974; Aoki & Kushiro, 1968; Becker, 1977; Boettcher & O'Neill, 1980; Ellis, 1976; Evans & Nash, 1979; Gianetti, 1982; Hunter et al., 1984; Sheraton & Cundari, 1980; Wilkinson, 1975.

Phenocrysts and groundmass in kimberlites and alkaline volcanics: Apter et al., 1984; Bachinski & Simpson, 1984; Baldridge et al., 1981; Barnett et al., 1984; Barton, 1979; Birch, 1978; Boctor & Boyd, 1982; Brooks et al., 1978;

Carmichael, 1967; Clarke et al., 1983; Cundari, 1975; Duda & Schmincke, 1978; Edgar, 1979; Elthon & Ridley, 1979; Furnes et al., 1982; Gupta & Yagi, 1980; Griffin & Taylor, 1975; Hall, 1982; Kuehner et al., 1981; Luhr & Carmichael, 1981; Mitchell, 1978, 1979, 1981; Mitchell & Meyer, 1980; Nielsen, 1980; Nixon, 1980; Platt & Mitchell, 1982; Rimsaite, 1971; Scott, 1979; Sheraton & Cundari, 1980; Smith et al., 1978; Thompson, 1977; Van Kooten, 1980; Wendlandt, 1977.

Melting experiments: Arima & Edgar, 1983a, b; Barton & Hamilton, 1979; Edgar et al., 1976, 1980.

Granulite facies rocks: Arima & Barnett, 1984; Clifford et al., 1981; Dymek, 1983; Ellis et al., 1980; Griffin et al., 1979; Grew, 1980; Hermans et al., 1976.

REFERENCES

Abrecht, J. & Hewitt, D.A. 1980: Ti-substitution in synthetic Fe-biotites. Geol. Soc. Am. Abstracts with Programs 12, 377.

Abrecht, J. & Hewitt, D.A. 1981: Substitutions in synthetic Ti-biotites. Geol. Soc. Am. Abstracts with Programs 13, 393.

Adams, G.E. & Bishop, F.C. 1982: Experimental investigation of Ca-Mg exchange between olivine, orthopyroxene, and clinopyroxene: potential for geobarometry. Earth Planet. Sci. Lett. 57, 241-250.

Anastasiou, P. & Seifert, F. 1972: Solid solubility of Al_2O_3 in enstatite at high temperatures and 1-5 kb water pressure. Contrib. Mineral. Petrol. 34, 272-287.

Aoki, K. 1974: Phlogopites and potassic richterites from mica nodules in South African kimberlites. Contrib. Mineral. Petrol. 48, 1-7.

Aoki, K. 1975: Origin of phlogopite and potassic richterite bearing peridotite xenoliths from South Africa. Contrib. Mineral. Petrol. 53, 145-156.

Aoki, K. & Kushiro, I. 1968: Some clinopyroxenes from ultramafic inclusions in Dreiser Weiher, Eifel. Contrib. Mineral. Petrol. 18, 326-337.

Apter, D.B., Harper, F.J., Wyatt, B.A. & Smith, B.H.S. 1984: The geology of the Mayeng kimberlite sill

complex, South Africa. In: Kornprobst, J. (ed.), Kimberlites, Vol. I. Elsevier, Amsterdam, 43-57.

Arai, S. 1984: Pressure-temperature dependent compositional variation of phlogopitic micas in upper mantle peridotites. Contrib. Mineral. Petrol. 87, 260-264.

Arima, M. 1978: Phase equilibria in the system $MgSiO_3$-Al_2O_3-Fe_2O_3 at high temperatures and pressures, with special reference to the solubility of Al_2O_3 and Fe_2O_3 in enstatite. J. Fac. Sci. Hokkaido Univ. Ser. IV, 18, 305-338.

Arima, M. & Barnett, R.L. 1984: Sapphirine bearing granulites from the Sipiwesk Lake area of the Late Archean Pikwitonei granulite terrain, Manitoba, Canada. Contrib. Mineral. Petrol. 88, 102-112.

Arima, M. & Edgar, A.D. 1981: Substitution mechanisms and solubility of titanium in phlogopites from rocks of probable mantle origin. Contrib. Mineral. Petrol. 77, 288-295.

Arima, M. & Edgar, A.D. 1983a: High pressure experimental studies on a katungite and their bearing on the genesis of some potassium-rich magmas of the west branch of the African Rift. J. Petrol. 24, 166-187.

Arima, M. & Edgar, A.D. 1983b: A high pressure experimental study on a magnesian-rich leucite lamproite from the West Kimberley area, Australia: petrogenetic implications. Contrib. Mineral. Petrol. 88, 228-234.

Bachinski, S.W. & Simpson, E.L. 1984: Ti-phlogopites of the Shaw's Cove minette: a comparison with micas of other lamprophyres, potassic rocks, kimberlites, and mantle xenoliths. Am. Mineral. 69, 41-56.

Bailey, D.K. 1982: Mantle metasomatism - continuing chemical change within the Earth. Nature 296, 525-530.

Bailey, S.W. 1984: Classification and structure of the micas. In: Bailey, S.W. (ed.), Reviews in Mineralogy, Vol. 13, Micas, Mineralogical Society of America, 1-12 (chapter 1).

Baldridge, W.S., Carmichael, I.S.E. & Albee, A.L. 1981: Crystallization paths of leucite-bearing lavas: examples from Italy. Contrib. Mineral. Petrol. 76, 321-335.

Barnett, R.L., Arima, M., Blackwell, J.D., Winder, C.G., Hayatsu, A. & Palmer, H.C. 1984/1985: The Picton and Varty lake ultramafic dikes, Jurassic magmatism in the St. Lawrence platform. Can. J. Earth Sci. 21, 1460-1472.

Barton, M. 1979: A comparative study of some minerals occurring in the potassium-rich alkaline rocks of the Leucite Hills, Wyoming, the Vico volcano, Western Italy, and the Toro-Ankole region, Uganda. N. Jb. Mineral. Abh. 137, 113-134.

Barton, M. & Hamilton, D.L. 1979: The melting relationship of a madupite from the Leucite Hills, Wyoming, to 30 kb. Contrib. Mineral. Petrol. 69, 133-142.

Becker, H.J. 1977: Pyroxenites and hornblendites from the maar-type volcanoes of Westeifel, Federal Republic of Germany. Contrib. Mineral. Petrol. 65, 45-52.

Birch, W.D. 1978: Mineralogy and geochemistry of the leucitite at Cosgrove, Victoria. J. Geol. Soc. Austr. 25, 369-385.

Boctor, N.Z. & Boyd, F.R. 1982: Petrology of kimberlite from the DeBruyn and Martin Mine, Bellsbank, South Africa. Am. Mineral. 67, 917-925.

Boettcher, A.L. & O'Neil, J.R. 1980: Stable isotope, chemical, and petrographic studies of high-pressure amphiboles and micas: evidence for metasomatism in the mantle source regions of alkali basalts and kimberlites. Am. J. Sci. 280A, 594-621.

Boettcher, A.L., O'Neil, J.R., Windom, K.E., Stewart, D.C. & Wilshire, H.G. 1979: Metasomatism of the upper mantle and the genesis of kimberlites and alkali basalts. In: Boyd, F.R. & Meyer, H.O.A. (eds.), The Mantle Sample: Inclusions in Kimberlites and other Volcanics. Am. Geophys. Union, 173-182.

Bohlen, S.R., Peacor, D.R. & Essene, E.J. 1980: Crystal chemistry of a metamorphic biotite and its significance in water barometry. Am. Mineral. 65, 55-62.

Bohlen, S.R., Wall, V.J. & Boettcher, A.L. 1984: Geobarometry in granulites. In: Saxena, S.K. (ed.), Kinetics and equilibrium in mineral reactions. Springer-Verlag New York, (Chapter 5), 141-171.

Boyd, F.R. & England, J.L. 1960: Apparatus for phase equilibrium measurements at pressures up to 50 kb and temperatures to 1750°C. J. Geophys. Res. 65, 741-748.

Brey, G. & Green, D.H. 1977: Systematic study of liquidus phase relations in olivine melilitite + H_2O + CO_2 at high pressures and petrogenesis of an olivine melilitite magma. Contrib. Mineral. Petrol. 61, 141-162.

Brooks, C.K., Noe-Nygaard, A., Rex, D.C. & Ronsbo, J.G. 1978: An occurrence of ultrapotassic dikes in the neighbourhood of Holsteinborg, West Greenland. Bull. Geol. Soc. Denmark, 27, 1-8.

Burns, R.G. & Dyar, M.D. 1984: Crystal chemistry of ferric micas. Geol. Soc. Am. Abstracts with Programs Ann. Meeting Reno, 459-460.

Burns, R.G. & Vaughan, D.J. 1975: Polarized electronic spectra. In: Karr, C. (ed.), Infrared and raman spectroscopy of lunar and terrestrial minerals. Academic Press, New York, 39-72.

Carmichael, I.S.E. 1967: The mineralogy and petrology of the volcanic rocks from the Leucite Hills, Wyoming. Contrib. Mineral. Petrol. 15, 24-66.

Carswell, D.A. 1975: Primary and secondary textured phlogopites and clinopyroxenes in garnet lherzolite xenoliths. Phys. Chem. Earth 9, 417-429.

Chopin, C. 1984: Coesite and pure pyrope in high-grade blueschists of the Western Alps: a first record and some consequences. Contrib. Mineral. Petrol. 86, 107-118.

Chopin, C. & Maresch, W.V. 1984: High-pressure metamorphism: indicator of subduction and crustal thickening. Terra Cognita 4, 33-34.

Clarke, D.B., Muecke, G.K. & Pe-Piper, G. 1983: The lamprophyres of Ubekendt Ejland, West Greenland: products of renewed partial melting or extreme differentiation. Contrib. Mineral. Petrol. 83, 117-127.

Clifford, T.N., Stumpfl, E.F., Burger, A.J., McCarthy, T.S. & Rex, D.C. 1981: Mineral-chemical and isotopic studies of Namaqualand granulites, South Africa: a Grenville analogue. Contrib. Mineral. Petrol. 77, 225-250.

Colby, J.W. 1971: Magic IV, a computer program for quantitative electron microprobe analysis. Bell Telephone Laboratories, Allentown, Pennsylvania.

Cundari, A. 1975: Mineral chemistry and petrogenetic aspects of Vico lavas, Roman Volcanic Region, Italy. Contrib. Mineral. Petrol. 53, 129-144.

Czamanske, G.K. & Wones, D.R. 1973: Oxidation during magmatic differentiation, Finnmarka Complex, Oslo Area, Norway: Part 2, The mafic silicates. J. Petrol. 14, 349-380.

Danchin, R.V. 1979: Mineral and bulk chemistry of garnet lherzolite and garnet harzburgite xenoliths from the Premier Mine, South Africa.. In: Boyd, F.R. & Meyer, H.O.A. (eds.), The mantle sample: inclusions in kimberlites and other volcanics. Am. Geophys. Union, 104-126.

Dankwerth, P.A. & Newton, R.C. 1978: Experimental determination of the spinel peridotite to garnet peridotite reaction in the system $MgO-Al_2O_3-SiO_2$ in the range 900°C-1100°C and Al_2O_3 isopleths of enstatite in the spinel field. Contrib. Mineral. Petrol. 66, 189-201.

Davis, B.T.C. & Boyd, F.R. 1966: The join $Mg_2Si_2O_6$-$CaMgSi_2O_6$ at 30 kilobars pressure and its application to pyroxenes from kimberlites. J. Geophys. Res. 71, 3567-3576.

Dawson, J.B. & Smith, J.V. 1973: Alkalic pyroxenite xenoliths from the Lashaine volcano, Northern Tanzania. J. Petrol. 14, 113-131.

Dawson, J.B. & Smith, J.V. 1975: Chemistry and origin of phlogopite megacrysts in kimberlite. Nature 253, 336-338.

Dawson, J.B. & Smith, J.V. 1977: The MARID (mica-amphibole-rutile-ilmenite-diopside) suite of xenoliths in kimberlite. Geochim. Cosmochim. Acta 41, 309-323.

Dawson, J.B & Smith, J.V. 1982: Upper-mantle amphiboles: a review. Mineral. Mag. 45, 35-66.

Dawson, J.B., Powell, D.G. & Reid, A.M. 1970: Ultrabasic xenoliths and lava from the Lashaine volcano, Northern Tanzania. J. Petrol. 11, 519-548.

Deer, W.A., Howie, R.A. & Zussman, J. 1965: Rock-Forming Minerals, vol. 3, Sheet Silicates. Longmans, London.

Delaney, J.S., Smith, J.V., Carswell, D.A. & Dawson, J.B. 1980: Chemistry of micas from kimberlites and xenoliths - II. Primary- and secondary-textured micas from peridotite xenoliths. Geochim. Cosmochim. Acta 44, 857-827.

Duda, A. & Schmincke, H.-U. 1978: Quarternary basanites, melilite nephelinites and tephrites from the Laacher Sea area (Germany). N. Jb. Mineral. Abh. 132, 1-33.

Dymek, R.F. 1978: Metamorphism of the Archaean Malene supracrustals, Godthåb district, West Greenland. In: Smith, I.M.E. & Williams, J.G. (eds.), Proceedings of the 1978 Archean Geochemistry Conference. University of Toronto Press, 339-342.

Dymek, R.F. 1983: Titanium, aluminum and interlayer cation substitutions in biotite from high-grade gneisses, West Greenland. Am. Mineral. 68, 880-899.

Edgar, A.D. 1979: Mineral chemistry and petrogenesis of an ultrapotassic-ultramafic volcanic rock. Contrib. Mineral. Petrol. 71, 171-175.

Edgar, A.D. & Arima, M. 1983: Conditions of phlogopite crystallization in ultrapotassic volcanic rocks. Mineral. Mag. 47, 11-19.

Edgar, A.D., Green, D.H. & Hibberson, W.O. 1976: Experimental petrology of a highly potassic magma. J. Petrol. 17, 339-356.

Edgar, A.D., Condliffe, E., Barnett, R.L. & Shirran, R.J. 1980: An experimental study of an olivine ugandite magma and mechanisms for the formation of its K-enriched derivatives. J. Petrol. 21, 475-497.

Ehrenberg, S.N. 1979: Garnetiferous ultramafic inclusions in minette from the Navajo Volc. Field. In: Boyd, F.R. & Meyer, H.O.A. (eds.), The Mantle Sample: Inclusions in Kimberlites and other Volcanics. Am. Geophys. Union, 330-344.

Ehrenberg, S.N. 1982: Petrogenesis of garnet lherzolites and megacrystalline nodules from the Thumb, Navajo Volcanic Field. J. Petrol. 23, 507-547.

Ellis, D.J. 1976: High pressure cognate inclusions in the Newer Volcanics of Victoria. Contrib. Mineral. Petrol. 58, 149-180.

Ellis, D.J. & Green, D.H. 1979: An experimental study of the effect of Ca upon garnet-clinopyroxene Fe-Mg

exchange equilibrium. Contrib. Mineral. Petrol. 71, 13-22.

Ellis, D.J., Sheraton, J.W., England, R.N. & Dallwitz, W.B. 1980: Osumilite-sapphirine-quartz granulites from Enderby Land, Antarctica - mineral assemblages and reactions. Contrib. Mineral. Petrol. 72, 123-143.

Elthon, D. & Ridley, W.I. 1979: The oxide and silicate mineral chemistry of a kimberlite from the Premier Mine: implications for the evolution of kimberlitic magmas. In: Boyd, F.R. & Meyer, H.O.A (eds.), Kimberlites, Diatremes and Diamonds. Their Geology, Petrology and Geochemistry. Am. Geophys. Union, 206-216.

Emeleus, C.H. & Andrews, J.R. 1975: Mineralogy and petrology of kimberlite dyke and sheet intrusions and included peridotite xenoliths from south-west Greenland. Phys. Chem. Earth 9, 179-197.

Engel, A.E.J. & Engel, C. 1960: Progressive metamorphism and granitization of the major paragneiss, northwest Adirondack Mountains, New York, Pt. 2. Mineralogy. Geol. Soc. Am. Bull. 71, 1-58.

Evans, S.H. & Nash, W.P. 1979: Petrogenesis of xenolith-bearing basalts from southeastern Arizona. Am. Mineral. 64, 249-267.

Evans, S. & Raftery, E. 1980: X-ray photoelectron studies of titanium in biotite and phlogopite. Clay Minerals

15, 209-218.

Exley, R.A., Sills, J.D. & Smith, J.V. 1982: Geochemistry of micas from the Finero spinel-lherzolite, Italian Alps. Contrib. Mineral. Petrol. 81, 59-63.

Farmer, G.L. & Boettcher, A.L. 1981: Petrologic and crystal-chemical significance of some deep-seated phlogopites. Am. Mineral. 66, 1154-1163.

Faye, G.H. 1968: The optical absorption spectra of iron in six coordinated sites in chlorite, biotite, phlogopite and vivianite. Some aspects of pleochroism in the sheet silicates. Can. Mineral. 10, 25-34.

Forbes, W.C. & Flower, M.F.J. 1974: Phase relations of titan-phlogopite, $K_2Mg_4TiAl_2Si_6O_{20}(OH)_4$: A refractory phase in the upper mantle? Earth Planet. Sci. Lett. 22, 60-66.

Foster, M.D. 1960a: Layer charge relations in the dioctahedral and trioctahedral micas. Am. Mineral. 45, 383-398.

Foster, M.D. 1960b: Interpretation of the compositions of trioctahedral micas. U.S. Geol. Surv. Prof. Paper 354-B, 11-48.

Furnes, H., Elvsborg, A. & Malm, O.E. 1982: Lower and Middle Jurassic alkaline magmatism in the Egersund sub-basin, North Sea. Marine Geol. 46, 53-69.

Gaspar, J.C. & Wyllie, P.J. 1982: Barium phlogopite from the Jacupiranga carbonatite, Brazil. Am. Mineral. 67,

997-1000.

Ghent, E.D. 1976: Plagioclase-garnet-Al_2SiO_5-quartz: a potential geobarometer-geothermometer. Am. Mineral. 61, 710-714.

Ghent, E.D. & Stout, M.Z. 1984: TiO_2 activity in metamorphosed pelitic and basic rocks: principles and applications to metamorphism in southeastern Canadian Cordillera. Contrib. Mineral. Petrol. 86, 248-255.

Gianetti, B. 1982: Cumulate inclusions from K-rich magmas, Roccamonfina volcano, Italy. Earth Planet. Sci. Lett. 57, 313-335.

Grew, E.S. 1980: Sapphirine + quartz association from Archean rocks in Enderby Land, Antarctica. Am. Mineral. 65, 821-836.

Green, T.H. 1982: Synthetic high-pressure micas compositionally intermediate between the dioctahedral and trioctahedral mica series. Contrib. Mineral. Petrol. 78, 452-458.

Griffin, W.L. & Heier, K.S. 1973: Petrological implications of some corona structures. Lithos 6, 315-335.

Griffin, W.L. & Taylor, P.N. 1975: The Fen damkjernite: petrology of a "central-complex kimberlite". Phys. Chem. Earth 9, 163-176.

Griffin, W.L., Carswell, D.A. & Nixon, P.H. 1979: Lower-crustal granulites and eclogites from Lesotho, southern Africa. In: Boyd, F.R. & Meyer, H.O.A. (eds.),

The Mantle Sample: Inclusions in Kimberlites and other Volcanics. Am. Geophys. Union, 59-86.

Griffin, W.L., Wass, S.V. & Hollis, J.D. 1984: Ultramafic xenoliths from Bullenmerri and Gnotuk Maars, Victoria, Australia: petrology of a sub-continental crust-mantle transition. J. Petrol. 25, 53-87.

Guidotti, C.V. 1984: Micas in metamorphic rocks. In: Bailey, S.W. (ed.), Reviews in Mineralogy, Vol. 13, Micas, Chapter 10, 357-467.

Guidotti, C.V., Cheney, J.T. & Guggenheim, S. 19??: Distribution of titanium between coexisting muscovite and biotite in pelitic schists from northwestern Maine. Am. Mineral. 62, 438-448.

Gupta, A.K. & Yagi, K. 1980: Petrology and Genesis of Leucite-Bearing Rocks. Springer-Verlag, Berlin, 252 pp.

Hall, A. 1982: The Pendennis peralkaline minette. Mineral. Mag. 45, 257-266.

Harley, S.L. 1984: An experimental study of the partitioning of Fe and Mg between garnet and orthopyroxene. Contrib. Mineral. Petrol. 86, 359-373.

Harley, S.L. & Green, D.H. 1982: Garnet-orthopyroxene barometry for granulites and peridotites. Nature 300, 697-701.

Harte, B. 1983: Mantle peridotites and processes - the kimberlite sample. In: Hawkesworth, C.J. & Norry,

M.J. (eds.), Continental Basalts and Mantle Xenoliths. Shiva Publishing, Cheshire.

Harte, B. & Gurney, J.J. 1975: Ore mineral and phlogopite mineralization within ultramafic nodules from the Matsoke kimberlite pipe, Lesotho. Carnegie Inst. Wash. Yb. 74, 528-536.

Hazen, R.M. & Wones, D.R. 1972: The effect of cation substitutions on the physical properties of tri-octahedral micas. Am. Mineral. 57, 103-129.

Hermans, G.A.E.M., Hakstege, A.L., Jansen, J.B.H. & Poorter, R.P.E. 1976: Sapphirine occurrence near Vikèsa in Rogaland, southwestern Norway. Norsk Geol. Tidsskr. 56, 397-412.

Herzberg, C.T. 1978: Pyroxene geothermometry and geo-barometry: experimental and thermodynamic evaluation of some subsolidus phase relations involving pyroxenes in the system $CaO-MgO-Al_2O_3-SiO_2$. Geochim. Cosmochim. Acta 42, 945-957.

Hewitt, D.A. & Wones, D.R. 1984: Experimental phase relations of the micas. In: Bailey, S.W. (ed.), Reviews in Mineralogy, Vol. 13, Micas, chapter 7, 201-256.

Holland, T.J.B. 1980: The reaction albite = jadeite + quartz determined experimentally in the range 600°C-1200°C. Am. Mineral. 65, 129-134.

Hunter, R.H., Kissling, R.D. & Taylor, L.A. 1984: Mid- to late-stage kimberlitic melt evolution: phlogopites and oxides from the Fayette County kimberlite, Pennsylvania. Am. Mineral. 69, 30-40.

Irving, A.J. & Frey, F.A. 1984: Trace element abundances in megacrysts and their host basalts: Constraints on partition coefficients and megacryst genesis. Geochim. Cosmochim. Acta 48, 1201-1221.

Johannes, W., Bell, P.M., Mao, H.K., Boettcher, A.L., Chipmann, D.W., Hays, J.F., Newton, R.C. & Seifert, F. 1971: An interlaboratory comparison of piston-cylinder pressure calibration using the albite break-down reaction. Contrib. Mineral. Petrol. 32, 24-38.

Johnson, C.A., Bohlen, S.R. & Essene, E.J. 1983: An evaluation of garnet-clinopyroxene geothermometry in granulites. Contrib. Mineral. Petrol. 84, 191-198.

Jones, A.P., Smith, JV. & Dawson, J.B. 1982: Mantle metasomatism in 14 veined peridotites from Bultfontein Mine, South Africa. J. Geol. 90, 435-453.

Kay, S.M., Snedden, W.T., Foster, B.P. & Kay, R.W. 1983: Upper mantle and crustal fragments in the Ithaca kimberlites. J. Geol. 91, 277-290.

Kuehner, S.M., Edgar, A.D. & Arima, M. 1981: Petrogenesis of the ultrapotassic rocks from the Leucite Hills, Wyoming. Am. Mineral. 66, 663-677.

Kunitz, W. 1936: Beitrag zur kenntis der magmatischen Assoziationex. III. Die Rolle des Titans und Zirkoniums in der gesteinbildenden Silikaten. N. Jb. Mineral. Geol. Palaont. 70, 385-416.

Leavy, B.D. 1979: Mantle xenoliths from southeastern New England. In: Boyd, F.R. & Meyer, H.O.A. (eds.), The Mantle Sample: Inclusions in Kimberlites and other Volcanics. Am. Geophys. Union, 374-381.

Lindsley, D.H. & Dixon, S.S. 1976: Diopside-enstatite equilibria at 850°C-1400°C, 5-35 kbar. Am. J. Sci. 276, 1285-1301.

Lloyd, F.E. & Bailey, D.K. 1975: Light element metasomatism of the continental mantle: the evidence and the consequences. Phys. Chem. Earth 9, 389-416.

Luhr, J.F. & Carmichael, I.S.E. 1981: The Colima volcanic complex, Mexico: Part II. Late-Quarternary cinder cones. Contrib. Mineral. Petrol. 76, 127-147.

MacGregor, I.D. 1974: The system $MgO-Al_2O_3-SiO_2$: solubility of Al_2O_3 in enstatite for spinel and garnet peridotite compositions. Am. Mineral. 59, 110-119.

McCulloch, M.T., Jacques, A.L., Nelson, D.R. & Lewis, J.D. 1983: Nd and Sr isotopes in kimberlites and lamproites from Western Australia: an enriched mantle origin. Nature 302, 400-403.

McIver, J.R. 1981: Aspects of ultrabasic and basic alkaline intrusive rocks from Bitterfontein, South

Africa. Contrib. Mineral. Petrol. 78, 1-11.

Mitchell, R.H. 1978: Mineralogy of the Elwin Bay kimberlite, Somerset Island, N.W.T., Canada. Am. Mineral. 63, 47-57.

Mitchell, R.H. 1979: Mineralogy of the Tunraq kimberlite, Somerset Island, N.W.T., Canada. In: Boyd, F.R. & Meyer, H.O.A (eds.), Kimberlites, Diatremes and Diamonds. Their Geology, Petrology and Geochemistry. Am. Geophys. Union, 161-171.

Mitchell, R.H. 1981: Titaniferous phlogopites from the leucite lamproites of the West Kimberley area, Western Australia. Contrib. Mineral. Petrol. 76, 243-251.

Mitchell, R.H. 1984: Garnet lherzolites from the Hanaus-I and Louwrensia kimberlites of Namibia. Contrib. Mineral. Petrol. 86, 178-188.

Mitchell, R.H. & Mayer, H.O.A. 1980: Mineralogy of micaceous kimberlite from the Jos Dyke, Somerset Island, N.W.T. Can. Mineral. 18, 241-250.

Modreski, P.J. & Boettcher, A.L. 1972: The stability of phlogopite + enstatite at high pressures: a model for micas in the interior of the Earth. Am. J. Sci. 272, 852-869.

Mori, T. 1978: Experimental study of pyroxene equilibria in the system CaO-MgO-FeO-SiO_2. J. Petrology 19, 45-65.

Mori, T. & Green, D.H. 1978: Laboratory duplication of phase equilibria observed in natural garnet lherzolites. J. Geol. 86, 83-97.

Newton, R.C. & Haselton, H.T. 1981: Thermodynamics of the garnet-plagioclase-Al_2SiO_5-quartz geobarometer. In: Newton, R.C., Navrotsky, A. & Wood, B.J. (eds.), Thermodynamics of minerals and melts. Springer-Verlag, Berlin, 129-145.

Newton, R.C. & Perkins, D. 1982: Thermodynamic calibration of geobarometers based on the assemblages garnet-plagioclase-orthopyroxene (clinopyroxene)-quartz. Am. Mineral. 67, 203-222.

Nickel, K.G. & Green, D.H. 1984: The nature of the uppermost mantle beneath Victoria, Australia, as deduced from ultramafic xenoliths. In: Kornprobst, J. (ed.), Kimberlites, Vol. II, 161-178.

Nielsen, T.F.D. 1980: The petrology of a melilitolite, melteigite, carbonatite and syenite ring dike system, in the Gardiner complex, East Greenland. Lithos 13, 181-197.

Nixon, P.H., Mitchell, R.H. & Rogers, N.W. 1980: Petrogenesis of alnoitic rocks from Malaita, Solomon Islands, Melanesia. Mineral. Mag. 43, 587-596.

Oba, T., Yagi, K. & Nicholls, I.A. 1984: The substitutions of $R^{2+}+2Si^{IV} = {}^{\square}Ti^{VI}2Al^{IV}$ and the dependence of Ti content on pressure in amphiboles. Extended

abstract. Workshop on Experimental Geochemistry, Monash University, Australia, Jan. 23-27, 1984. Wall, V.J. & Nicholls, I.A. (convenors).

Otten, M.T. 1984: Ti substitution in hornblende and biotite: an electron energy-loss spectroscopic study. Geol. Soc. Am. Abstracts with Programs 16, 615-616.

Pasteris, J.D. 1981: Kimberlites: strange bodies? Eos 62, 713-718.

Pasteris, J.D. 1984: Kimberlites: complex mantle melts. Ann. Rev. Earth Planet. Sci. 12, 133-153.

Perkins, D. & Newton, R.C. 1980: The composition of co-existing pyroxenes and garnet in the system CaO-MgO-Al_2O_3-SiO_2 at 900-1100°C and high pressures. Contrib. Mineral. Petrol. 75, 291-300.

Platt, R.G. & Mitchell, R.H. 1982: The Marathon dikes: ultrabasic lamprophyres from the vicinity of McKellar Harbour, N.W. Ontario. Am. Mineral. 67, 907-916.

Prinz, M., Manson, D.V., Hlava, P.F. & Keil, K. 1975: Inclusions in diamonds: garnet lherzolite and eclogite assemblages. Phys. Chem. Earth 9, 797-815.

Radoslovich, E.W. & Norrish, K. 1962: The cell dimensions and symmetry of layer-lattice silicates. I. Some structural considerations. Am. Mineral. 47, 599-616.

Raheim, A. & Green, D.H. 1974: Experimental determination of the temperature and pressure dependence of the Fe-Mg partition coefficient for coexisting garnet and

clinopyroxene. Contrib. Mineral. Petrol. 48, 179-203.

Richardson, S.W., Bell, P. & Gilbert, M.C. 1968: Kyanite-sillimanite equilibrium between 700°C and 1500°C. Am. J. Sci. 266, 513-541.

Rimsaite, J. 1971: Distribution of major and minor constituents between mica and host ultrabasic rocks, and between zoned mica and zoned spinel. Contrib. Mineral. Petrol. 33, 259-272.

Robert, J.L. 1976: Titanium solubility in synthetic phlogopite solid solutions. Chem. Geol. 17, 213-227.

Ross, M., Huebner, J.S. & Dowty, E. 1973: Delineation of the one atmosphere augite-pigeonite miscibility gap for pyroxenes from lunar basalt 12021. Am. Mineral. 58, 619-635.

Ryabchikov, I.D. & Green, D.H. 1978: The role of carbon dioxide in the petrogenesis of highly potassic magmas. In: Problems of Petrology of the Earth's Crust and Mantle. Issue 403, Nauka, Novosibirsk. Trans. Inst. Geol. Geofiz. Akad.

Scott, B.H. 1979: Petrogenesis of kimberlites and associated potassic lamprophyres from central west Greenland. In: Boyd, F.R. & Meyer, H.O.A. (eds.), Kimberlites, Diatremes and Diamonds: Their Geology, Petrology and Geochemistry. Am. Geophys. Union, 190-205.

Scott Smith, B.H. & Skinner, E.M.W. 1984: A new look at Prairie Creek, Arkansas. In: Kornprobst, J. (ed.), Kimberlites, Vol. I, Elsevier, Amsterdam, 255-283.

Sekine, T. & Wyllie, P.J. 1982a: Phase relationships in the system $KAlSiO_4$-Mg_2SiO_4-SiO_2-H_2O as a model for hybridization between hydrous siliceous melts and peridotite. Contrib. Mineral. Petrol. 79, 368-374.

Sekine, T. & Wyllie, P.J. 1982b: The system granite-peridotite-H_2O at 30 kbar, with applications to hybridization in subduction zone magmatism. Contrib. Mineral. Petrol. 81, 190-202.

Sekine, T. & Wyllie, P.J. 1982c: Synthetic systems for modeling hybridization between hydrous siliceous magmas and peridotite in subduction zones. J. Geol. 90, 734-741.

Sekine, T. & Wyllie, P.J. 1983: Experimental simulation of mantle hybridization in subduction zones. J. Geol. 91, 511-528.

Sheraton, J.W. & Cundari, A. 1980: Leucitites from Gaussberg, Antarctica. Contrib. Mineral. Petrol. 71, 417-427.

Smith, C.B. 1983: Pb, Sr and Nd isotopic evidence for sources of southern African Cretaceous kimberlites. Nature 304, 51-54.

Smith, J.V., Brennesholtz, R. & Dawson, J.B. 1978: Chemistry of micas from kimberlites and xenoliths -

I. Micaceous kimberlites. Geochim. Cosmochim. Acta 42, 959-971.

Smith, J.V., Kervig, R.L., Ackermand, D. & Dawson, J.B. 1979: K, Rb and Ba in micas from kimberlite and peridotitic xenoliths, and implications for origin of basaltic rocks. In: Boyd, F.R. & Meyer, H.O.A. (eds.), Kimberlites, Diatremes and Diamonds: Their Geology, Petrology and Geochemistry. Am. Geophys. Union, 241-251.

Smith, J.V., Delaney, R.L., Hervig, R.L. & Dawson, J.B. 1981: Storage of F and Cl in the upper mantle: geochemical implications. Lithos 14, 133-147.

Thompson, R.N. 1977: Primary basalts and magma genesis. III. Alban Hills, Roman comagmatic province, central Italy. Contrib. Mineral. Petrol. 60, 91-108.

Van Kooten, G.K. 1980: Mineralogy, petrology and geochemistry of an ultrapotassic basaltic suite, central Sierra Nevada, California, U.S.A. J. Petrol. 21, 651-684.

Wells, P.R.A. 1977: Pyroxene thermometry in simple and complex systems. Contrib. Mineral. Petrol. 62, 129-139.

Wendlandt, R.F. 1977: Barium phlogopite from Haystack Butte, Highwood Mountains, Montana. Carnegie Inst. Wash. Yb. 76, 534-539.

Wendlandt, R.F. & Eggler, D.H. 1980a: The origins of potassic magmas: 1. Melting relations in the systems $KAlSiO_4$-Mg_2SiO_4-SiO_2 and $KAlSiO_4$-MgO-SiO_2-CO_2 to 30 kilobars. Am. J. Sci. 280, 385-420.

Wendlandt, R.F. & Eggler, D.H. 1980b: The origins of potassic magmas: 2. Stability of phlogopite in natural spinel lherzolite and in the system $KAlSiO_4$-MgO-SiO_2-H_2O-CO_2 at high pressures and high temperatures. Am. J. Sci. 280, 421-458.

Wilkinson, J.F.G. 1975: An Al-spinel ultramafic-mafic inclusion suite and high pressure megacrysts in an analcimite and their bearing on basaltic magma fractionation at elevated pressures. Contrib. Mineral. Petrol. 53, 71-104.

Wones, D.R., Burns, R.G. & Caroll, B.M. 1971: Stability and properties of synthetic annite. Am. Geophys. Union. Trans. 52, 369.

Wood, B.J. 1974: The solubility of alumina in orthopyroxene coexisting with garnet. Contrib. Mineral. Petrol. 46, 1-15.

Wood, B.J. & Banno, S. 1973: Garnet-orthopyroxene and orthopyroxene-clinopyroxene relationships in simple and complex systems. Contrib. Mineral. Petrol. 42, 109-121.

Wyllie, P.J. 1979: Magmas and volatile components. Am. Mineral. 64, 469-500.

Wyllie, P.J. & Sekine, T. 1982: The formation of mantle phlogopite in subduction zone hybridization. Contrib. Mineral. Petrol. 79, 375-380.

Yoder, H.S. & Kushiro, I. 1969: Melting of a hydrous phase: phlogopite. Am. J. Sci. 267A, 558-582.

END

12/11/85

FIN